A Density Functional Theory Study of Methanol Synthesis Catalysed by Gold

By

Noko S. Phala

B.Sc (Chemical Engineering) – University of Cape Town

Submitted in partial fulfilment of the requirements for the degree of

Master of Science in Engineering

February 2002

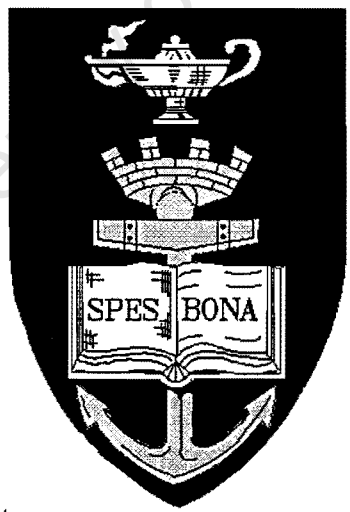

Catalysis Research Unit
Department of Chemical Engineering
University of Cape Town
Private Bag
Rondebosch, 7701
South Africa

SYNOPSIS

Methanol synthesis is one of the most efficient gas to liquid conversion technologies available today. Synthesis gas, a $CO/CO_2/H_2$ mixture, can be converted to methanol over a fixed bed of catalyst at temperatures around 250°C and pressures exceeding 50 atmospheres. The reactions involved are exothermic and they occur with a decrease in the number of moles. Therefore, high pressures and low temperatures are required to obtain thermodynamically favourable yields. In the light of the diminishing oil reserves, improvements in the methanol synthesis technology are the focus of many syngas research groups. Catalysts that are active at low temperatures are required, as these will enable the use of low pressures without compromising the methanol yield.

Even though methanol synthesis has been in existence for many decades, there are conflicting views on the mechanism of methanol synthesis over the commercial Cu/ZnO catalysts. Surface techniques employed for identification of surface species cannot distinguish between species which are *actively* involved in the synthesis, and those that are mere "spectators". There is also debate on the active valence state of the catalytically active material. Reaction mechanisms is an area of catalytic chemistry where theory can provide useful insights.

Ab initio Molecular Orbital calculations by Kakumoto (1995) suggested that bridged formate (*OCHO*) and methoxy (CH_3O*) species are the active species involved in methanol synthesis over copper catalysts. The positive partial charge on copper suggested that cationic copper is the active valence state of the catalyst, supporting an experimental deduction by Klier *et al.* (1982).

On the other hand, Frost (1988) suggested that the function of the metal is to promote the productivity of the oxide support. As a result, the metal should have a high enough workfunction to enhance the equilibrium concentration of oxygen vacancies on the oxide, through formation of a Schottky barrier with the oxide conduction band. Although some researchers do not accept this hypothesis (e.g. Shaw *et al.*, 1992), it enabled prediction of the methanol synthesis activity for gold, a metal with superior catalytic activity for CO oxidation (Haruta *et al.*, 1989). The methanol synthesis activity for gold was achieved when gold was deposited onto basic metal oxide supports, e.g. ZnO, as small particles, such that the interfacial contact perimeter distance between the gold particles and the support is maximised (Sakurai and Haruta, 1996). Investigating the mechanistic aspects of this recently found gold catalysts was the subject of this dissertation.

A probable reaction mechanism on Au/ZnO catalysts was determined via calculations based on Density Functional Theory, with corrections for relativity using effective core potentials. The energy levels of various probable intermediates bound to gold and zinc atoms were computed. The calculations were also performed over copper atoms, for comparison. Single metal atoms were used to appropriate the catalytic centre.

While the mechanism over a Cu/ZnO catalyst was found to involve a methoxy species (CH_3O^*), in agreement with Kakumoto's results (1995), a mechanism involving a hydroxymethyl (CH_2O^*H) species was found to be of low energy over gold. Zinc sites were found to be capable of methanol formation through the methoxy route. Gold (and all the other metals) had a positive partial charge in the minimum energy structures. This implied that for gold catalysts, Au^+ will be the active site for methanol synthesis. Au^0 might be required for adsorption of reactants. A redox mechanism for the generation of cationic species under catalytic conditions, where the Au^+/Au^0 ratio is determined by the CO_2/CO ratio of the feed, was proposed. The theory can explain why small gold particles are desired, because they oxidise easily.

The distribution of electron density on an Au_7 cluster, representing two adjacent four-fold follow sites of an Au (111) surface, was calculated to identify an active centre. All atoms were on one plane. It was found that the atoms on the outer layer were metallic or slightly anionic, while the central atom had a positive charge. If cationic gold atoms are the active sites, then the centre atom is the active centre. When two oxygen atoms were placed above the Au_7 cluster, to form an Au_7O_2 cluster, the partial charge on the active centre increased from 0.39 to 0.57, clearly indicating that interaction of a gold surface with an oxidant will increase its catalytic activity, if cationic sites are the active sites.

To investigate the effect of adjacent ZnO entities on the charge distribution of the gold cluster, ZnO entities replaced the Au atoms of the Au_7 cluster, to form models of $Au_6(ZnO)$ and $Au_5(ZnO)_2$ clusters. The resultant distribution of electron density indicated that ZnO induces electronic effects onto the gold surface, making the gold centre more cationic. On the basis of these findings, a hypothetical "$Au^{\delta+}$-O-Me^+" interface model was proposed, where the function of Me is to increase the effective charge on gold, which is why choice of the support oxide is also very important.

ACKNOWLEDGEMENTS

Many people contributed to the existence of this thesis. It is, indeed, a great pleasure to thank them in this dedicated section.

I am indebted to Assoc. Prof. Jack Fletcher, who basically created this opportunity for me, and gave me continuous guidance throughout this work.

The enthusiastic supervision of Prof. Eric van Steen is highly acknowledged. His inspiration and efforts to simplify complex concepts for me made quantum chemistry and metal catalysis very interesting topics to learn.

I owe a great deal to Dr Günter Klatt, who introduced me to molecular modelling. I particularly thank him for the many nights and weekends that he spent taking care of my computing problems. Many thanks for the technical inputs as well.

I am grateful to the entire Catalysis Research group, for creating a work environment that basically makes learning fun. My coworkers' assistance with all types of problems - technical or domestic - is highly appreciated.

I wish to thank my employers at AngloGold for presenting this career development opportunity to me. Special thanks go to Mr Peter Radcliffe and Mr Greg Donoghue for their guidance. I thank AngloGold also for their financial support.

I would like to thank my brothers, sisters, uncles, grandparents, aunts, cousins, and friends for their support and encouragement.

Finally, and most importantly, I wish to thank my parents, Mamorei and Mosebjadi, for believing in me. Their unconditional love was always there when I needed it most. I dedicate this thesis to them.

TABLE OF CONTENTS

LIST OF FIGURES

LIST OF TABLES

SYMBOLS

α	Constant determining the radial extent of a Gaussian-type orbital
C_i	Coefficient for the expansion of a molecular orbital describing electron, i.
c	Velocity of light
E	Energy
$F[\rho(r)]$	Density functional that yields the sum of the kinetic energy of the electrons and the contribution from the electron self-interactions
ϕ	Basis set, or one electron wavefunction, used to build molecular orbital wavefunctions
ΔG_{RXN}	Free energy change for a reaction
γ	Parameter describing the extent of pertubation of the Hartree-Fock Hamiltonian
ΔH_{RXN}	Heat of formation for a reaction
H	Hamiltonian operator
P	Pressure
$\rho(r)$	Electron density at point, r
T	Temperature
V	Pertubation, the difference between a Hamiltonian for the true solution of the Schrödinger equation and a Hamiltonian derived from the Hartree-Fock solution

V_{ext}	External potential field
v	Velocity
ψ	Wavefunction, which gives information about the motion of the particles that it describes
ζ	Constant determining the size of a Slater-type orbital

ACRONYMS

B3LYP	Hybrid Becke, Lee, Yang and Parr density functional method, with DFT and HF exchange functionals
CI	Configuration Interaction
CISD	Configuration Interaction with Single and Double excitations
DFT	Density Functional Theory
ECP	Effective Core Potential
EDX	Energy Dispersive X-ray Analysis
EELS	Electron Energy Loss Spectrometry
FCC	Face-Centred Cubic cell
FT-IR	Fourier-Transform Infrared Spectroscopy
GAMESS	General Atomic and Molecular Electronic Structure System
GHSV	Gas Hourly Space Velocity
GTO	Gaussian-type orbital
HCP	Hexagonal closed packing
HF	Hartree-Fock ab initio method
IR	Infrared Spectroscopy

LanL2DZ	Hay-Wadt valence double zeta basis, with an ECP for core electrons
MP	Møller-Plesset pertubation theory
SA	Surface Area
STO	Slater-type orbital
TEM	Transmission Electron Microscopy
TOF	Turnover Frequency
TPD	Temperature Programmed Desorption
TPR	Temperature Programmed Reduction
UHF	Unrestricted Hartree-Fock method
UV-VIS	Ultraviolet Visible Spectroscopy
XPS	X-ray Photoelectron Spectroscopy
XRD	X-ray Diffraction

1 INTRODUCTION

1.1 Background

Methanol synthesis is the hydrogenation of carbon oxides (CO and CO_2) to methanol, over metal catalysts. The reaction is exothermic, and occurs with a decrease in the number of moles. Conditions that favour high thermodynamic yield are, thus, low temperature and high pressure.

Synthetic methanol production first began in 1923 at BASF's Leuna Plant, Germany, using a zinc-chromium oxide based catalyst. The activity of the catalyst required it to be operated at 250-350 bar and 320-450°C, resulting in high capital and compression costs (English *et al.*, 1992). ICI introduced the low-pressure (50 – 100 bar) methanol synthesis technology in 1966 over a copper/zinc oxide/alumina catalyst operating at *ca.* 250°C (Bart and Sneeden, 1987). ICI uses a series of adiabatic beds with interbed cooling by injection of cold synthesis gas to obtain high conversion per pass. The life of a methanol synthesis catalyst is typically two years (Chinchen *et al.*, 1988).

Feedstocks for industrial methanol synthesis over copper catalysts consist of synthesis gas that contains H_2, CO, CO_2 and traces of inert methane (Bart and Sneeden, 1987). Synthesis gas derived from steam reforming of natural gas has typical composition of 73%H_2, 15%CO, 9%CO_2 and 3%CH_4 (English *et al.*, 1992). There are large quantities of carbon sources on earth that can be converted into useful chemicals. Methanol synthesis remains as one of the efficient methods of converting natural carbon sources to liquids, in addition to Fischer-Tropsch synthesis, and will hence remain economically important to countries with large natural carbon sources.

Presently, the largest use of methanol is in the production of formaldehyde, about 40% of the market. Other major markets include its use in the synthesis of methyl t-butyl ether (MTBE), an oxygen additive for petrol, and acetic acid (English *et al.*, 1992).

Japan and the United States are currently developing new methanol uses as fuels for automobiles, and in fuel cells (Weirauch, 1998 and Dolan, 2001). These potential future applications are expected to cause a large-scale demand for methanol. Attempts to increase the efficiency of the methanol synthesis reaction through the search for more active catalysts will, thus, remain relevant.

The South African economy is modern, sophisticated and based firmly on manufacturing, mining and agriculture (Solomon, 1992). For over a century, gold has dominated South Africa's mining sector and economy, holding about half of the world's known gold reserves. Sadly, future growth of the gold industry is expected to be at a lower rate due to the decreased exploration as a result of the depressed gold prices. An immediate challenge for gold producing companies is to aim at stabilising the gold price. A logical way of achieving this is to diversify the application of the metal. From an economic point of view, it is essential that gold's potential as a catalyst for important industrial and environmental reactions be explored.

1.2 Thermodynamics of Methanol Synthesis

Table 1.1 shows the reactions that occur during methanol synthesis. For thermodynamic calculations, only two of the three reactions shown in Table 1.1 form a pair of independent reactions. The methanol synthesis reactions are exothermic and occur with a decrease in the number of moles. Therefore methanol yield is favoured by conditions of low temperature and high pressure. Figure 1.1 shows the thermodynamic yield of methanol as a function of temperature for a typical feed to a methanol synthesis reactor. Yield is defined as the number moles of methanol formed per mole of carbon in the starting material. Selectivity is typically greater than 99%. Typical impurities are ethers, esters, aldehydes, ketones, higher alcohols and waxes.

Table 1.1: Methanol synthesis reactions.

Reactions			$\Delta H_{RXN,\ 25°C}$ (kJ/mol)[1]	$\Delta G_{RXN,\ 25°C}$ (kJ/mol)[1]
$CO + 2H_2$	=	CH_3OH	-91	-25
$CO_2 + 3H_2$	=	$CH_3OH + H_2O$	-49	+3.3
$CO_2 + H_2$	=	$CO + H_2O$	+41	+29

[1]Calculated using the CHEMEQ program in Sandler (1999)

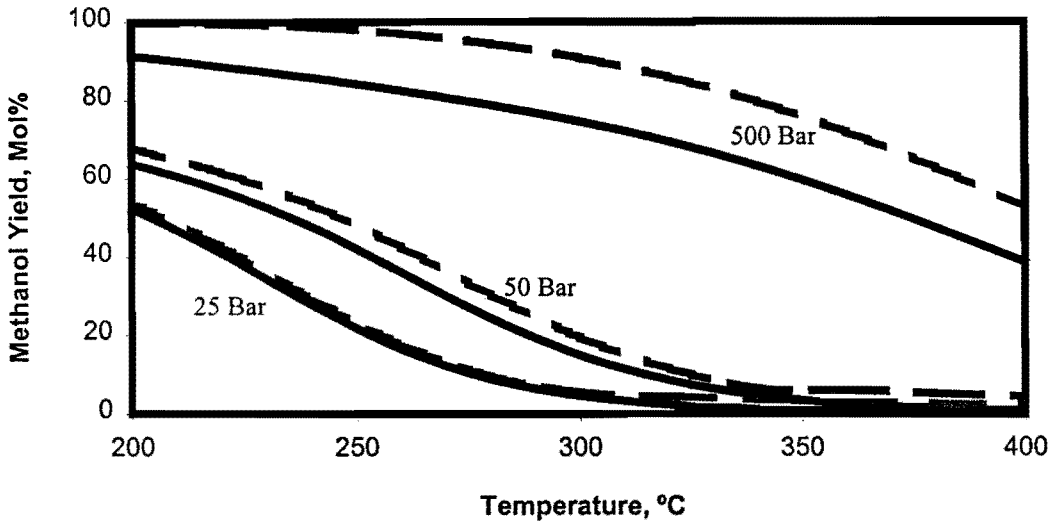

Figure 1.1: Equilibrium yield of methanol (mol %) as a function of temperature. H_2/C = 3:1, and CO_2/CO = 2:3. Yield is defined as the moles of methanol formed per mole of carbon in the starting material. Dashed lines indicate corrections to account for non-idealities of the system, using the Peng-Robinson equation of state (Sandler, 1999).

Correcting for the non-idealities of the system gives higher yields than when the corrections are not made. This is because the fugacity coefficients of the products, H_2O and CH_3OH, are much less than unity, while the fugacity coefficients for the reactants, CO, CO_2 and H_2, approach unity. This is more evident in the high pressure region.

Figure 1.2 shows the effect of CO_2 content of the feed on the thermodynamic yield of methanol. Corrections for non-idealty were not performed, as deviations from ideality at 50 bar are relatively small (see Figure 1.1). CO_2 suppresses the thermodynamic yield of methanol, since hydrogenation of CO_2 is thermodynamically more limited than hydrogenation of CO. At 25°C, the Gibbs' free energy of methanol formation from CO_2 is 3.3 kJ/mol, and –25 kJ/mol for methanol formation from CO. Despite this thermodynamic limitation, methanol synthesis is typically carried out in the presence of carbon dioxide, for kinetic reasons (Bart and Sneeden, 1987).

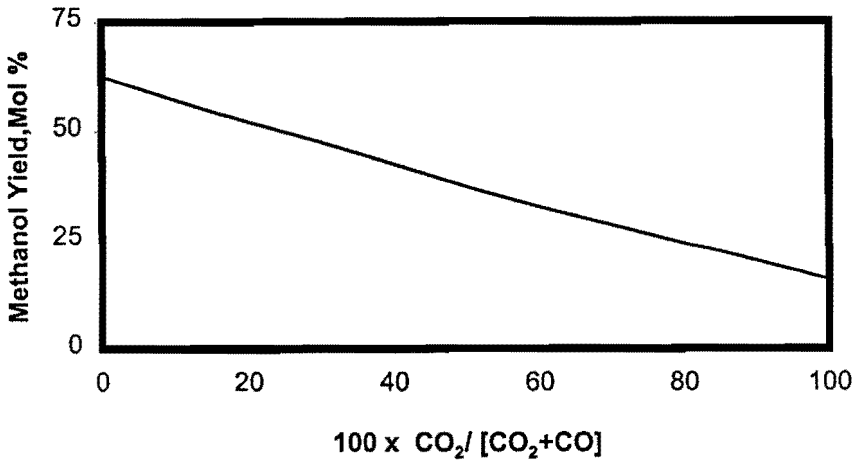

Figure 1. 2: Equilibrium yield of methanol (mol%) as a function of the CO_2 content, using ideal gas approximation. $H_2/C = 3:1$, P = 50 bar and T = 250 °C. Yield is defined as the moles of methanol formed per mole of carbon in the starting material.

1.3 Copper-Catalysed Methanol Synthesis

1.3.1 Preparation of the Commercial $Cu/ZnO/Al_2O_3$ Catalysts

The industrial catalyst, $Cu/ZnO/Al_2O_3$, is typically prepared by a coprecipitation technique (Bart and Sneeden, 1987). This involves addition of salts of the catalyst components to a sodium carbonate solution at temperatures between 60 and 80°C, at a pH of 7. A precipitate, which is a mixture of malachite ($Cu_2(OH)_2CO_3$), roderite ($(Cu, Zn, Al)_5(OH)_6(CO_3)_2$),and rosasite ($(Cu, Zn)_2(OH)_2CO_3$), is formed. This precipitate is washed with copious amounts of water, to remove sodium, and is subsequently calcined in air at about 350°C. Before use, the resultant oxides are reduced in H_2 at 240°C to transfer the catalyst into its active form.

A novel method of preparing active Cu/Zn/Al catalysts is the oxalate gel coprecipitation method, used by Zhang *et al.* (1997). In this method, oxalic acid and mixed salts of copper nitrate, zinc nitrate and aluminium nitrate (molar ratio Cu:Zn:Al = 60:30:10) were dissolved in ethanol. The ethanol solution of oxalic acid was rapidly added to the mixed solution of metal nitrates at 25°C under vigorous stirring. A gel-like precipitate was formed and separated by centrifuge. The precipitate was either

dried without washing at 110°C under flowing air, or washed with de-ionised water or ethanol before drying. The subsequent treatments hereafter were the same as for the normal coprecipitation method. Catalysts prepared in this manner had copper particles with diameter between 11 and 30nm.

1.3.2 Effect of Feed Composition on the Reaction Rate

Typical feedstocks for the industrial methanol synthesis consist of mixtures of CO_2, CO and H_2, even though CO_2 hydrogenation is thermodynamically more limited than CO hydrogenation. Early workers observed that methanol synthesis from a pure CO_2 feed occurred with different activity and selectivity to that from pure CO feed under similar catalytic systems (Ramaroson *et al.*, 1982).

In oxygen labelling experiments at 220°C and about 16 bar, Liu *et al.* (1985) observed that the rate of formation of $CH_3{}^{18}OH$ was comparable to the rate of formation of $CH_3{}^{16}OH$ when the ratio of the oxides in the feed was $C^{18}O_2/C^{16}O$ = 1/20. This suggested that CO_2 hydrogenation is much faster than CO hydrogenation. This was later confirmed by Fisher *et al.* (1997), who found that over a Cu/ZrO_2 catalyst, the apparent activation energy for methanol synthesis from CO at 6.5 bar was 73 kJ/mol, while for methanol synthesis from CO_2 under the same conditions the apparent activation energy was 55 kJ/mol. This suggests that CO_2 can be hydrogenated at lower temperatures than CO. Zhang *et al.* (1997) have shown that a synergy seems to exist in $CO/CO_2/H_2$ mixed feeds, since the methanol synthesis rates for the individual CO and CO_2 hydrogenations are much lower than for CO/CO_2 mixture hydrogenation over the same temperature range (see Figure 1.3).

On the observation that small amounts of CO_2 promote the methanol synthesis reaction, Klier *et al.* (1982) studied methanol yield for different CO_2/CO ratios over a Cu/ZnO catalyst prepared by a coprecipitation technique. As shown in Figure 1.4, the addition of very small amounts of CO_2 clearly promotes the steady state yield of methanol, and increased amounts results in a decline in the yield of methanol.

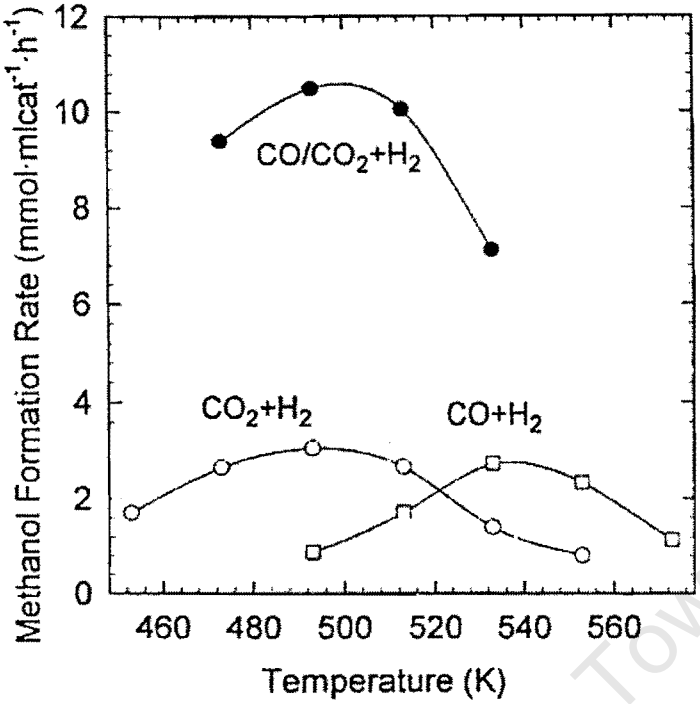

Figure 1.3: Effect of temperature on the methanol synthesis rate for CO/H_2 = 1/2, CO_2/H_2 =1/3, $CO:CO_2:H_2$ = 20.5:5:74.5. P =20 bar, GHSV = 4500 h^{-1}, over a Cu/Zn/Al catalyst prepared via an oxalate gel coprecipitation method (Zhang *et al.*, 1997).

The authors stated that while CO_2 might increase the rate of methanol formation due to creation of active catalyst oxidation state, the yield will go down at higher CO_2 dosages due to equilibrium limitations. Their explanation for the decline in conversion does not seem to be valid since it can be clearly seen in Figure 1.4 that the conversion declines while it is still significantly far from equilibrium. The same group of workers noticed a promotional effect of other oxidising agents on methanol synthesis rate. They report rate enhancement effects upon co-feeding traces of O_2 and H_2O to the feed (Herman *et al.*,1979).

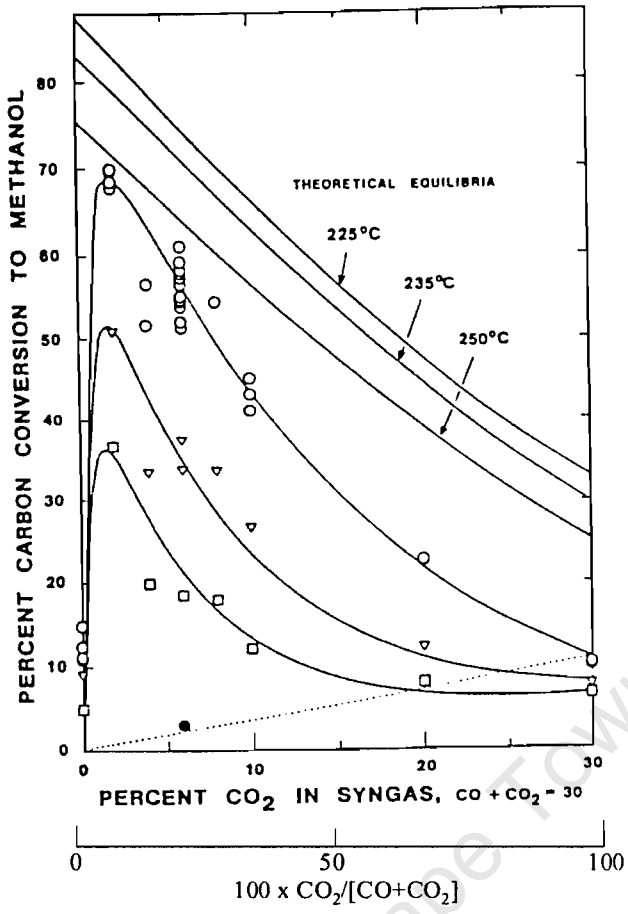

Figure 1.4: Effect of CO_2 content of feed gas on the yield of methanol. P=75 atm; GHSV = 6100 ml/g/hr, 70% H_2 + 30% (CO + CO_2) (Klier *et al.*, 1982). Data are shown for 250°C(○), 235°C(▽), and 225°C(□). ● denotes the yield in CO_2/Ar/H_2=6/24/70 gas, expressed in terms of equivalent conversion of (CO_2 + Ar) to methanol.

Liu *et al.* (1984) measured the initial rate of methanol synthesis in a batch reactor as a function of the CO_2 content of the feed over the range studied by Klier *et al.* (1982). They observed that the initial rate of formation of methanol increased monotonously with an increase in the content of CO_2 (see Figure 1.5), which seemed to contradict the findings by Klier *et al.* (1982) in a flow reactor who observed a maximum in the activity as a function of CO_2 content. These authors stated that their results, since they measured differential conversion, represent a true indication of the CO_2 effect, without the water effects. They concluded that CO_2 generally increases the reaction rate, but water, which gets formed at high conversions attainable in an integral

reactor, promotes the reverse reaction to CO_2 and H_2, thus reducing the methanol formation rate. Various authors (e.g. Takawaga and Ohsugi,1987 and Sahibzada *et al*, 1998) have since reproduced both Klier's and Liu's results and arrived at the conclusion that water inhibits the synthesis rate by promoting the reverse reactions.

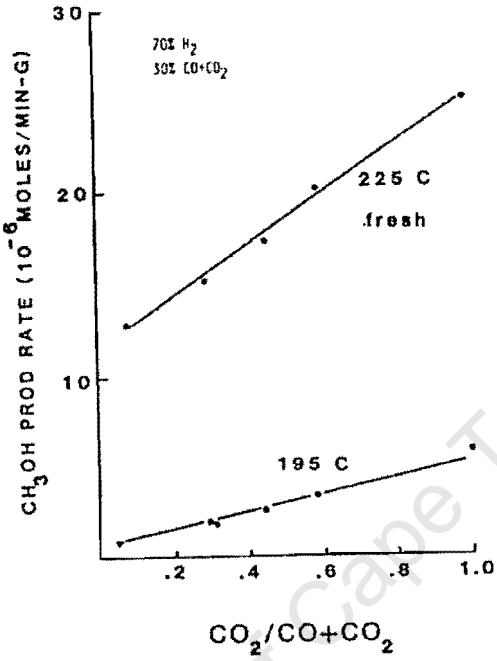

Figure 1.5: Effect of the CO_2 concentration in the synthesis gas on the initial rates of methanol production. P = 17 atm, synthesis gas is 70%H_2 + 30% (CO + CO_2). Data at 225°C were for a fresh catalyst, while data at 195°C were for a steady state catalyst. Cu/ZnO catalyst (Liu *et al.*, 1984).

That water inhibits the reaction at high CO_2 conversion is an experimental fact, in the light of the different results obtained at differential and finite conversions (Takawaga and Ohsugi,1987 and Sahibzada *et al.*, 1998, Klier *et al.*, 1982, Liu *et al.*, 1984). But the cause of the inhibition is unlikely to be as stated by the authors due to the fact the decline in conversion occurs very far from equilibrium, and that traces of water and oxygen increased the reaction rate (Herman *et al.*, 1979). An alternative explanation should be sought.

1.3.3 The Active State of the Catalyst

The results discussed in the context of feed composition suggest that an oxidising atmosphere is essential for high catalytic activity. Fujitani *et al.* (1994) measured the specific activity of methanol synthesis from CO_2 over various metal oxides (see Figure 1.6). It was found that the aerial rate increased with increasing oxygen coverage, until an oxygen coverage of 0.17, after which the reaction rate declined with increasing oxygen coverage. The use of an aerial rate justified comparison of the different catalysts, as it ruled out the possibility that the observed effect was due to the difference in the surface areas of the catalysts.

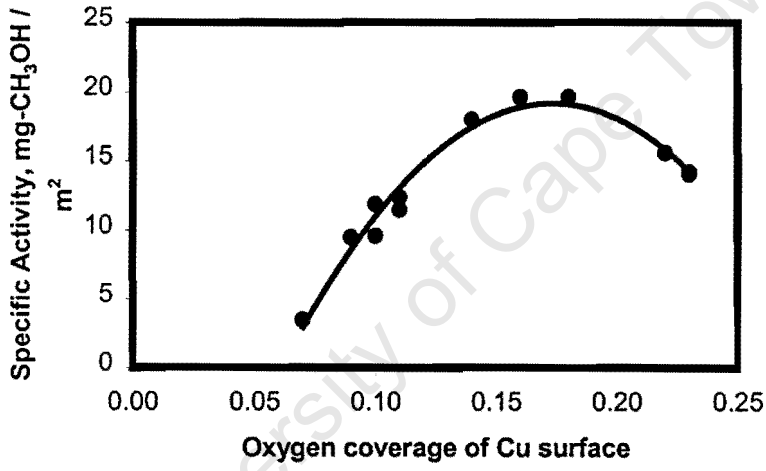

Figure 1.6: Rates of methanol synthesis over copper catalysts supported on different metal oxides (Fujitani *et al.*, 1994). The coverage by oxygen was obtained via an N_2O titration technique. Conditions: T=250°C, H_2/CO_2 =3, P=50 bar.

In another study by the same group of workers (Nakamura *et al.*, 1995), methanol was produced over a Zn-deposited polycrystalline copper surface at 18 bar and 250°C from a CO_2/H_2 feed. Turnover frequency (TOF) increased with increasing Zn coverage (θ_{Zn}) on Cu until at $\theta_{Zn} = 0.17$, after which TOF declined with Zn coverage. Post-reaction surface analysis by XPS revealed the presence of oxygen on the catalyst model. The surface coverage by oxygen was found to be exactly the same as the

coverage by Zn up to the Zn coverage of 0.4, suggesting the formation of ZnO on the Cu surface. Comparison of the binding energy peaks before and after reaction suggested the formation of Cu^+, which was not necessarily associated with CuO. It was, thus, postulated that the oxygen was more strongly bonded to Zn than Cu, and this produced a Cu^+-O-Zn^{n+} ($1<n<2$) species, which could be the active site in methanol synthesis. Therefore, there should be an optimum Cu^+/Cu^0 ratio because TOF decreased at high coverages of zinc (and hence oxygen) on the model surface. The role of Cu^0 could simply be to dissociate H_2.

The theory of the simultaneous requirement of Cu^0 and Cu^+ can explain the results by Klier *et al.* (1982) without resorting to the reverse methanol depletion reaction. As the CO_2 content increases, the Cu^+ content also increases due to the redox reaction:

$$2Cu + CO_2 = Cu_2O + CO \qquad (1.1)$$

At too high CO_2 levels, most of the Cu^0 ,which is also required to supply H_2, gets depleted, hence the decline in activity. An optimum CO_2/CO ratio is thus required to attain a certain Cu^+/Cu^0 ratio. In an integral reactor, the optimum Cu^+/Cu^0 ratio is reached quicker than in a differential reactor because the water formed by the reverse water-gas shift reaction also converts the Cu^0 to Cu^+ according to the redox:

$$2Cu + H_2O = Cu_2O + H_2 \qquad (1.2)$$

In a differential reactor, the Cu^+/Cu^0 might not even reach its maximum value due to the absence of water. Hence the monotonous increase in rate with the CO_2 content (Liu *et al.*, 1984).

In the absence of CO_2 as an oxidising agent (as in methanol synthesis with pure CO), migration of ZnO to copper metal will be a necessity if $Cu^{\delta+}$ is indeed the active catalyst state. Kanai *et al.* (1994) suggested, through EDX, TPD, XRD and FT-IR studies, that ZnO_x species migrate from ZnO to Cu particles during H_2 reduction to form a Cu-Zn alloy. The lattice constant of Cu increased from 3.625 to 3.670 Å with increasing reduction temperature. Since the lattice constant of Cu-Zn alloy is greater

than that of Cu, the increase in the lattice constant was attributed to the formation of a Cu-Zn alloy, and hence oxidised copper. This result showed that active Cu^+ can indeed be generated during the reduction process in the absence of an oxidising agent in the feed.

1.3.4 Surface Species

Surface species reported in literature based on XPS, EELS, UV-VIS and IR spectroscopy include: adsorbed hydrogen (H*), adsorbed oxygen (O*), surface hydroxyl (OH*), adsorbed carbon monoxide (CO*), and formate (HCOO*) (Bart and Sneeden, 1987). Furthermore, identification of formate and methoxy (CH_3O*) species by chemical trapping technique has led to the postulate that formate, methylenedioxy (*OCH_2O*), and methoxy groups are reaction intermediates bonded through oxygen to a metal site (Bart and Sneeden, 1987). It should, however, be noted that nearly all experimental techniques are not able to differentiate between spectator and reactive surface species, and some species could have extremely low residence time on the surface and consequently be difficult to detect, even though they might be directly involved in the synthesis. Also, the relevance of *ex situ* techniques is debatable as the surface composition is being measured at conditions very far from those under which the reaction proceeds.

Jung and Bell (2000) performed *in situ* infrared studies of methanol synthesis over Cu/ZrO_2 catalyst at around 250°C and 6.5 bar. Bidentate formate on ZrO_2 (b-HCOO-Zr) and methoxy on ZrO_2 (CH_3O-Zr) were observed as strong peaks. Low intensity bands assignable to monodentate carbonate (m-CO_3-Zr), bidentate bicarbonate on ZrO_2 (b-HCO_3-Zr) and ionic carbonate (I-CO_3^{2-}) were observed. The formate, methoxy and bicarbonate species on Zr were also observable on ZrO_2 without copper. However, the rates of formation of these intermediates were 500-900 times faster on Cu/ZrO_2 than on ZrO_2 alone, when CO_2 is used. The rate of formate formation was, however, slower on Cu/ZrO_2 than on a ZrO_2 surface for CO hydrogenation. Over $Cu/ZrO_2/SiO_2$, mono- and bi-dentate formates on different sites (b-HCOO-Cu, m-HCOO-Cu and b-HCOO-Zr) could be differentiated. When the reaction was stopped, peaks assignable to b-HCOO-Cu decreased in intensity, while those assignable to b-

HCOO-Zr increased in intensity, suggesting the migration of formate species from Cu to Zr.

The rate at which Zr-OH groups undergo H/D exchange was found to be extremely fast for Cu/ZrO_2 in comparison to ZrO_2, suggesting spillover of atomic H from Cu to Zr. The metal dissociatively adsorbs H_2 (or D_2), and the atoms then spill over to the oxide surface.

A formaldehyde-type of species (CH_2O*) is often speculated as an intermediate in methanol synthesis, even though evidence for its existance is very indirect. Bowler *et al.* (1988) showed that adsorption of formaldehyde and methanol onto polycrystalline copper at 167°C produced the same stable formate species. Clearly, this result does not prove that formaldehyde forms before methanol. Formate can easily result from formaldehyde and methanol via different routes.

Sun *et al.*(1998) performed an extensive TPR-IR study on the mechanism of methanol synthesis over an ultrafine $Cu/ZnO/Al_2O_3$ catalyst. For CO_2/H_2 feed, CO peaks were observed at room temperature. With increasing temperature, CO peaks decreased in intensity, while those for H_2O and m-HCOO* increased in intensity. As the temperature was increased to 323 K, the peaks due to b-CO_3^{2-} increased in intensity, and then declined. Peaks due to b-HCOO* were observed at 313 K, and they reached steady state at 413 K. Meanwhile, the peaks assignable to CH_3O* and CH_3OH, which were not observed at lower temperatures, increased in intensity up to a temperature of 433 K. These results suggest that methanol is formed directly from CO_2 via a bi-dentate formate species, and a mono-dentate formate species, which should form methanol when starting from CO, does not exist at the same temperature as the methoxy and methanol entities. Methanol formation from CO is, thus, not a favourable route.

Although many workers support the existence of formate and methoxy species, the species that is formed after hydrogenation of formate, prior to methoxy formation, is not very well described. In one of the three mechanisms that they briefly presented, Duprez *et al.* (1990) presented a mechanism in which a mono-dentate formate, an

oxycarbinol ($OHCH_2O^*$) and a methoxy species are key intermediates in the synthesis (see Figure 1.7). The mechanism requires the presence of surface OH groups for initiation, obtained from the water that is released in the last step. This mechanism could explain the promotional effect of CO_2: it supplies water via the reverse water-gas shift reaction.

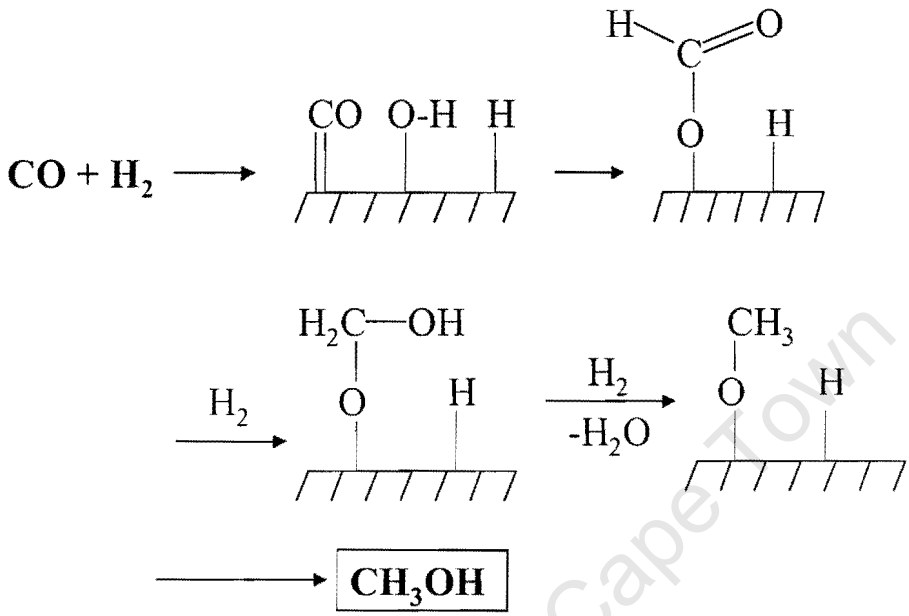

Figure 1.7: A reaction scheme for methanol synthesis proposed by Duprez *et al.*, 1990.

1.3.5 Insights from Theoretical Calculations

Ab initio molecular orbital calculations by Kakumoto (1995) suggested that the intermediates involved in methanol synthesis are probably bridged formate, formaldehyde, and methoxy species (see Figure 1.8). They performed calculations for a large number of intermediates (over twenty) at the MP4 level of theory, and found that these intermediates had the lowest energies compared with other possible intermediates. The species were bonded on Cu^+, suggesting that cationic copper is the active catalyst state. The stability of formate and formaldehyde species increased with increasing charge on copper, while that for the methoxy species was constant between Cu^0 and $Cu^{0.4+}$, and unstable above that level (Kakumoto and Watanabe, 1997). Carbonyl and formyl species were stable on Cu^0.

Hu *et al.* (1999) performed an ab initio study on the mechanism of methanol synthesis using a $Cu_8(6,2)$ cluster, which contained six atoms in the first layer and two atoms in the second layer, and arrived at a similar mechanism for the synthesis, only with an additional species, dioxomethylene (*OCH_2O*), located between the formate and the formaldehyde species. This species was, however, not observed when a theoretical study of a methoxy radical reversal to formaldehyde on a Cu (111) surface was conducted, even with clusters containing up to 22 atoms (Gomes *et al.*, 1999).

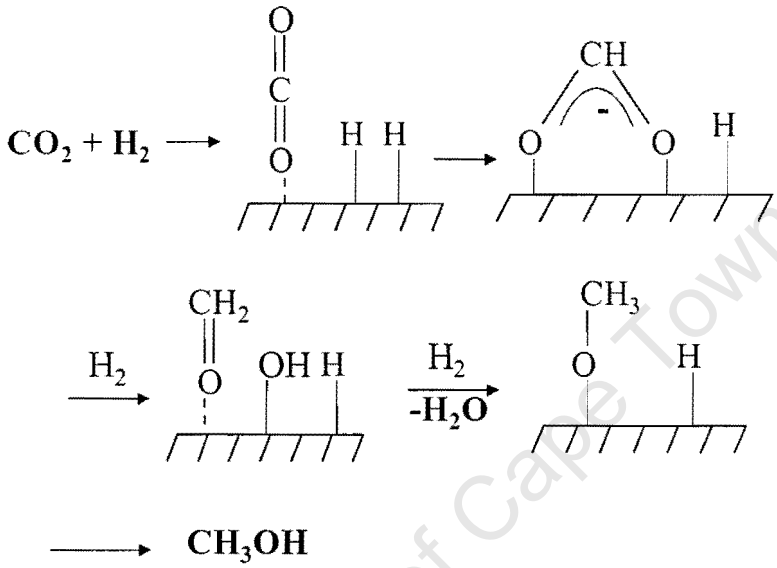

Figure 1.8: A reaction scheme for methanol synthesis from CO_2 hydrogenation (Kakumoto, 1995).

1.4 A Relatively New Catalyst: Gold

1.4.1 Earlier Findings

Research into the potential of gold as a catalytically active material was historically not extensive due to its chemical inertness, and hence its status as an investment item and a monetary unit. A review by Bond (1972) indicated that gold could not act as a hydrogenation or an oxidation catalyst in the normal sense because it adsorbed neither hydrogen nor oxygen at ambient temperatures. Schwank (1983), however, reported that formation of atomic hydrogen on gold surfaces occurs at 200°C, and gold catalysed the isotopic exchange reaction between hydrogen and deuterium above that

temperature. This result indicated the capability of gold to act as hydrogen transfer catalyst, once activated.

1.4.2 Recent Findings

Haruta and his co-workers (1989) were the first to show that gold-based catalysts have remarkable activity for oxidation of both carbon monoxide and hydrogen when prepared by special methods other than the conventional impregnation technique used to prepare platinum-group metal catalysts. Gold catalysts were prepared by coprecipitation from an aqueous solution of chloroauric acid and nitrates of various transition metals. Gold was dispersed on to the oxide supports as nanoparticles (diameters of 1.5 to 8 nm). Since then, suitably supported gold nanoparticles were found to have appreciable activity for a number of reactions of environmental and industrial interest. These include, *inter alia*, oxidation of methane (Waters *et al.*, 1995), epoxidation of propene (Hayashi *et al.*, 1998), reduction of nitric oxide (Ueda and Haruta, 1999), water-gas shift (Andreeva *et al.*, 1996), and methanol synthesis (Sakurai *et al.*, 1993).

1.5 Gold as a Methanol Synthesis Catalyst

1.5.1 A Prediction of Gold's Activity

Frost (1988) suggested that in methanol synthesis, the function of the metal is to promote the productivity of the oxide, and its surface chemistry is of little importance, as long as the metal work function is large enough to form a Schottky barrier with the oxide conduction band. In this view of the catalyst functioning, the active sites are thought to be the oxygen vacancies created on the oxide when electrons flow from the valance band to the conduction band. By forming a Schottky junction with the oxide conduction band, electrons at the conduction band can lower their energy by moving to the metal Fermi level. This results in a decrease in the enthalpy of formation of the oxygen vacancies. The equilibrium concentration of these oxygen vacancies will, thus, be higher. The work functions of Ag, Cu and Au are 4.26, 4.65 and 5.10 eV, respectively. Therefore, Ag and Au should, like Cu, be able to promote methanol synthesis on metal oxides, because the work functions are only 0.4 eV apart. With this theory, Frost (1988) was able to prepare active methanol synthesis catalysts from

silver and gold supported on the oxides of zinc, zirconium and thorium. Although Frost's theory is not without controversy (e.g. Shaw *et al.*, 1992), it enabled prediction of catalytic activity of gold for methanol synthesis.

1.5.2 Preparation of Gold Catalysts

The normal impregnation method used for preparing noble metal catalysts cannot lead to high dispersion of gold particles on the support. The size distribution is not narrow even at low metal loadings, ranging from small clusters to relatively large particles. Haruta *et al.* (1993) prepared supported gold catalysts for low-temperature oxidation of CO by coprecipitation. In this method, an aqueous mixture of $HAuCl_4$ and a nitrate of the corresponding metal oxide support was poured into an aqueous solution of Na_2CO_3. The precipitate was washed and then dried under vacuum overnight and finally calcined in air at 400°C for 5 hrs. Gold catalysts prepared in this manner had an average gold particle size of less than 4 nm on Fe_2O_3 and ZnO supports (Sakurai and Haruta, 1995).

Another preferred method for the preparation of gold catalysts is the deposition-precipitation method (Haruta *et al.*, 1993). In this method, a powder of the oxide support is mixed with appropriate amounts of aqueous solutions of $HAuCl_4$ at a fixed pH from 7 to 10. The slurry is then aged for 1 hr, after which it is washed with distilled water, decanted and the procedure repeated six times. The resulting material is vacuum-dried at 0.4 Pa and calcined in air at 400°C for 4 hrs. The catalysts are typically reduced in H_2 at 450°C for 10 hrs, even though this step is not necessary in some cases (Bamwenda *et al.*, 1997). Catalysts prepared in this method can have average gold particle sizes of around 2.9-3.5 nm, depending on the gold loading. Deposition-precipitation is not only preferred because it produces metallic gold particles with a narrow size distribution, but also because it prevents the copresence of the rafts of gold clusters, which were often observed in coprecipitated samples (Haruta *et al.*, 1993).

An alternative method to the liquid-phase methods of preparing gold catalysts is the chemical vapour deposition method. In this method, an organic gold precursor,

$(CH_3)_2Au(CH_3COCH_2COCH_3)$, is placed in a vessel and heated to 33°C to gradually evaporate the amount of a complex. The precursor adsorbed on the metal oxide supports that are mounted in the reaction vessel. The agglomerate is then calcined in air at a fixed temperature in the range of 200 – 500°C (Okumura *et al.*, 1998). Gold particles prepared this way had diameters ranging from 3.5 to 6.6 nm.

1.5.3 Interaction of Gold with Species Relevant to Methanol Synthesis

For gold to be active in methanol synthesis, interaction of gold clusters with CO, CO_2, H_2, and with potential surface intermediates, should be energetically favourable.

Interaction of Gold with CO and CO_2

The ability of gold to catalyse reactions involving both CO and CO_2 was investigated in the early days by Cha and Parravano (1970), who studied the redistribution of a carbon tracer between CO and CO_2 over Au/MgO catalysts at 300 to 400°C, i.e.

$$*CO_2(g) + CO(g) = CO_2(g) + *CO(g). \quad (1.3)$$

A CO_2/ CO/ $*CO_2$ feed mixture was used in the study. They observed an increase in activity of the catalyst with gold loading up to 2wt% gold, above which the rate was lower. The activity was found to decrease with an increasing CO_2/CO ratio, suggesting that reduced particles might have a specific role in the reaction.

The interaction of CO with supported gold particles is energetically favourable, as evidenced by gold's remarkable activity for CO oxidation (Haruta, 1997). Supported gold is the catalyst of choice for this reaction, being active at temperatures as low as –76°C and having turnover frequencies exceeding $0.1s^{-1}$ at 0°C (see Figure 1.9). At 0°C, the adsorption of CO on Au/TiO_2 was found to be reversible, and it followed the Langmuir isotherm (Iizuka *et al.*, 1997). The amount of CO adsorbed per unit total catalyst surface area was found to be similar to that of a gold powder. The result does not enable distinction of the adsorption sites for CO in gold catalysts, i.e. whether CO adsorbs onto the surface of gold, the support, or the interface, although Haruta (1997) proposes that it might be adsorbing on the interface. It is suggested that metallic gold

surfaces could be the CO adsorption sites (Haruta and Daté, 2001). Direct studies on the interaction of gold catalysts with CO_2 have not been reported.

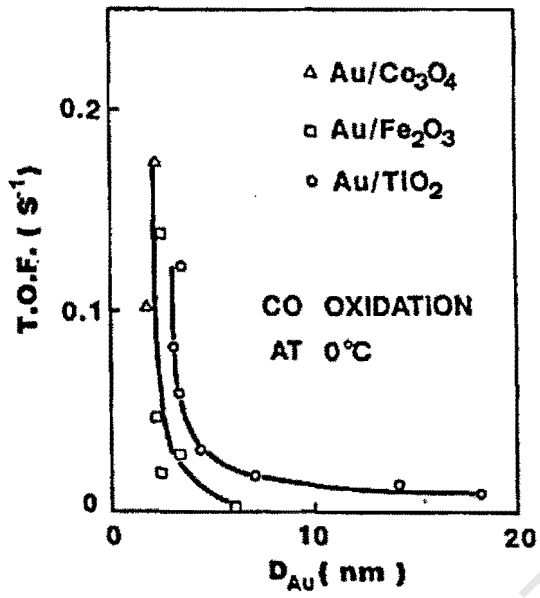

Figure 1.9: Turnover frequencies for CO oxidation at 0°C over supported gold catalysts, as a function of the mean diameter of the gold particles (Haruta *et al.*, 1993, 1997). 1%CO in air, GHSV = 20 000 ml/hr/g_{cat}. Unspecified pressure.

Interaction of Gold with H_2

In his review, Schwank (1983) mentioned that gold catalysed the isotopic exchange reaction between hydrogen and deuterium above 200°C. Furthermore, atomic hydrogen adsorbs on thin gold films at a temperature of –195°C (Stobinski *et al.*, 1996, 1997). These results suggest that gold can act as a hydrogen transfer catalyst.

Strømsnes *et al.* (2001) studied theoretically the dissociative chemisorption of molecular hydrogen on the Au (100) surface using a seven-atom cluster to describe the surface. All the atoms were in one plane, modelling two adjacent four fold hollow sites. The inter-atomic distances in the cluster were fixed at their bulk values. A relativistic effective core potential was used for all gold atoms, to take into account the relativistic effects which seem to dominate the chemistry of gold (Bartlett, 1998 and Bond, 2000). The process appeared to be endothermic, with the Au_7H_2 minimum

lying 79 kJ/mol above the ground state of the separated system of the gold cluster and H_2. An atomic chemisorption energy of 176 kJ/mol was predicted.

Interaction of Gold with Surface Species

A methoxy species has been speculated as a precursor to methanol in methanol synthesis. Gomes and Gomes (2000a) studied the adsorption of a methoxy radical on Cu, Ag and Au (111) surfaces using density functional theory. A 6-31G** basis set was used for the main-group elements, while an effective core potential basis by Hay and Wadt (1985) was used for the transition metals. The top, bridge, and hollow (FCC and HCP) sites of the M_7 clusters were modelled (see Figure 1.10). It was found that for Cu and Ag, the sequence of stability of the methoxy radical was top < bridge < hcp < fcc.

For gold, however, the adsorption energies for the bridge and the hollow sites were found to be similar. The adsorption energy, defined as the energy of the M_7OCH_3 entity minus the energy of the free methoxy and cluster entities, decreased in the group from copper to gold. For example, the adsorption energy for the top side, in kJ/mol, was -155.6, -103.3 and –6.9 for Cu, Ag and Au respectively. Adsorption energy of a formyl species (HC*O), which can form during CO hydrogenation, was found to be lower on an Au (111) surface than on Cu (111) and Pt (111) surfaces using the cluster approach (Gomes and Gomes, 2000b). The distance from the metallic surface to the carbon atom was largest for gold.

Recent DFT studies by Okumura *et al.* (2001) have shown that the outermost atoms in Au_{13} and $Au_{13}O_2$ clusters are negatively charged. This implies that in reactions where positively gold atoms are active sites, as could be during methanol synthesis, electronic modification of the cluster will be necessary. In a catalytic system, the modification could be via electronic effects induced by the support, or by interaction with an oxidant present in the feed.

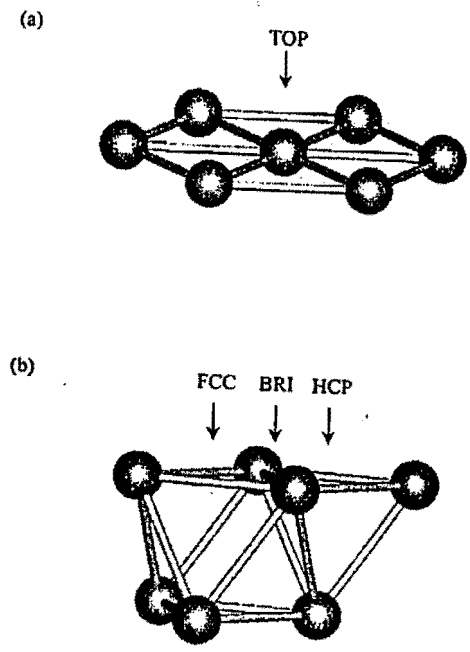

Figure 1.10: The seven atom cluster representation of the adsorption sites on the metal surface. (a) Top site, (b) bridge and hollow sites (Gomes and Gomes, 2000a).

1.5.4 Methanol Synthesis over Supported Gold Catalysts

Baiker *et al.* (1993) studied the hydrogenation of CO_2 over copper, silver and gold catalysts supported on zirconia at a total pressure of 17 bar. It was found that the catalytic behaviour of Ag/ZrO_2 and Cu/ZrO_2 catalysts were similar, and it contrasted the behaviour observed for Au/ZrO_2. The gold-based catalyst was active but its methanol yield was lower than that for copper and silver. Baiker *et al.* (1993) did not compare activities using the second extreme, i.e. pure CO feed. The same group of workers also succeeded in synthesizing methanol from CO_2/H_2 feed over an amorphous $Au_{25}Zr_{75}$ alloy (Koeppel *et al.*, 1991). On the basis of their experience with Pd/ZrO_2 and Cu/ZrO_2 catalysts, they assigned some vibrational bands on the alloy spectra to methoxy (CH_3O^*), formate ($HCOO^*$), carbonates (CO_3^{2-*}), and formaldehyde (CH_2O^*) as intermediates in the methanol synthesis.

Sakurai and Haruta (1993, 1995) investigated the hydrogenation of carbon monoxide and carbon dioxide over gold supported on titanium, iron and zinc oxides. Their

results are shown in Tables 1.2 and 1.3 for CO and CO_2 hydrogenation respectively. It can be seen from the tables that at the same conversion, the more basic the support, the higher is the methanol productivity, resulting in the activity order Au/ZnO >Au/Fe_2O_3 >Au/TiO_2. Over all the catalysts tested, carbon dioxide could be hydrogenated at lower temperatures than carbon monoxide, a result similar to the one obtained for Cu/ZnO catalyst. At 250°C, Au/ZnO gave higher methanol productivity than Cu/ZnO for methanol synthesis from CO, but the Cu/ZnO catalyst had superior activity for CO_2 hydrogenation. The Au/Fe_2O_3 catalyst had an intermediate productivity.

Table 1.2: Activity of gold catalysts for CO hydrogenation (Sakurai and Haruta, 1995). $CO/H_2/Ar = 30/60/10$, P = 50 atm, GHSV=3000 ml / h /g_{cat}.

Catalysts	d_{Au}, nm	SA, m^2/g	T,°C	CO conv, %	Product Selectivities[1] ,%		
					MeOH	CO_2	CH_4
Au/ZnO	3.5	41.0	250	3.7	70.3	29.7	0.3
			300	9.3	81.7	10.8	4.3
			400	17.5	4.0	47.4	42.3
Au/Fe_2O_3	3.3	32.8	250	9.8	16.3	54.1	13.3
			300	79.6	2.5	54.4	20.7
			400	88.8	0.1	52.0	18.7
Au/TiO_2	NR[2]	41.0	250	17.2	0.6	52.3	40.7
			300	65.3	0.2	53.3	34.5
			400	88.4	0.0	46.9	38.9
Cu/ZnO	NR	49.1	250	2.5	72.0	24.0	0.8
			300	10.3	81.6	11.7	3.9
			400	17.5	4.0	47.4	38.3
Cu/ZnO/Al_2O_3 (commercial)	NR	54.2	250	28.5	89.5	8.1	0.4
			300	26.0	45.3	36.5	3.1
			400	26.3	2.7	49.8	30.8

[1]Rest contained mainly C_2 to C_3 hydrocarbons, and unspecified products

[2]Not reported

Table 1.3: Activity of gold catalysts for CO_2 hydrogenation (Sakurai and Haruta, 1995). $CO_2/H_2/Ar = 23/67/10$, P = 50 atm, GHSV=3000 ml/ h/g_{cat}.

Catalysts	d_{Au} ,nm	SA,m^2 /g	T,°C	CO_2 conv, %	Product Selectivities[1] ,%		
					MeOH	CO	CH_4
Au/ZnO	3.5	41.0	250	8.2	48.8	51.2	0.0
			300	24.5	21.2	78.8	0.0
			400	37.7	1.1	98.4	0.5
Au/ZnO	33.9	NR[2]	250	0.0	-	-	-
(impregnation)			300	0.2	100	0.0	0.0
			400	3.7	32.4	56.8	5.4
Au/Fe_2O_3	3.3	32.8	250	18.4	29.3	69.6	1.1
			300	25.3	14.2	78.3	7.5
			400	38.3	0.8	67.1	32.4
Au/Fe_2O_3	NR	NR	250	12.4	31.5	68.5	0.0
(2^{nd} rxn cycle)			300	24.3	13.6	77.8	8.2
			400	40.0	0.0	40.5	38.5
Au/TiO_2	3 - 4	41.0	250	18.6	6.5	75.3	18.3
			300	25.6	1.2	58.6	39.8
			400	38.8	0.3	47.6	52.4
Au/$ZnFe_2O_4$	2.8	54.7	250	4.2	64.3	35.7	0.0
			300	20.1	24.4	74.6	1.0
			400	34.7	0.0	40.6	28.8
Cu/ZnO	NR	49.1	250	17.2	37.2	62.8	0.0
			300	25.3	16.6	83.0	0.01
			400	39.0	1.3	97.9	0.8
Cu/ZnO/Al_2O_3	NR	54.2	250	22.8	51.3	48.7	0.0
(commercial)			300	26.6	17.3	82.7	0.4
			400	38.1	1.3	94.2	3.4

[1]Rest contained mainly C_2 to C_3 hydrocarbons, and unspecified products

[2]Not reported

Sakurai and Haruta (1996) also investigated the particle size effect in methanol synthesis from CO_2. A series of Au/ZnO catalysts of different diameters were prepared and tested at 250°C and 300°C. It was found that the aerial methanol formation rate increased with a decreasing particle diameter (see Figure 1.11). Reduction of particle size is clearly related to creation of special sites, because the aerial rate of methanol formation did not remain constant (as one would expect from a dispersion effect). The authors explained that the special sites are located at the interface, because reduction of particle size results in an increase in the distance of the interface perimeter, because small particles were not fully spherical, but hemi-spherical. The nature of this synergy at the gold-support interface was, however, not clarified.

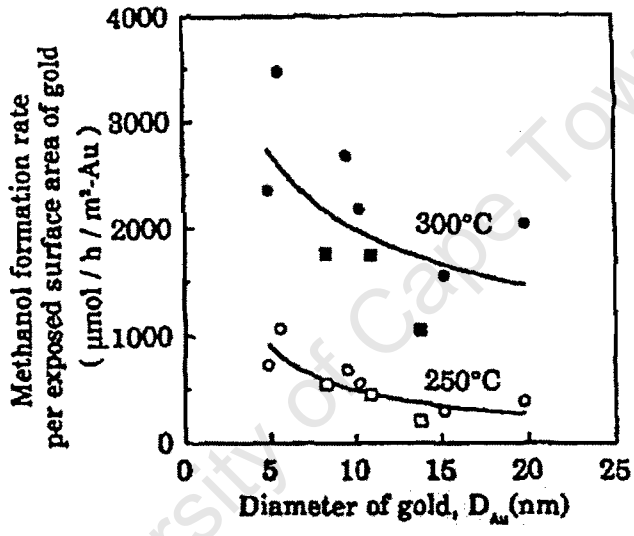

Figure 1.11: The aerial rate of methanol synthesis as a function of the mean diameter of the gold particles in Au/ZnO catalysts. The mean diameters were determined by TEM (●, ○) and XRD (■, □) (Sakurai and Haruta, 1996). $CO_2/H_2/Ar = 23/67/10$, P = 50 atm, GHSV=3000 ml/ h/g_{cat}.

1.6 Project Objectives

The literature provides evidence for the special requirement of Cu^+ for catalytic activity in methanol synthesis, with Cu^0 being required for adsorption of some of the feed components, most likely H_2. A "Cu^+-O-Zn^{n+}" type of interface was proposed, suggesting an active role of the support (Nakamura *et al.*, 1995). When coupled with

the recent finding that a synergy exists at the Au/MeO interface for gold catalysts, it is probable that small particles at the interface exist as Au^+, in a manner proposed for copper catalysts. A hypothesis is, thus, drawn:

'An active "Au^+-O-Me^{n+}" type of interface is created in Au/MeO methanol synthesis catalysts, which is why particles giving the largest interfacial contact distance give the highest activity in methanol synthesis'

The existence of such an interface raises a few issues. Firstly, the species involved in methanol synthesis over Au/MeO catalysts should be stable on cationic gold, as opposed to metallic gold. Secondly, as oxidants seem to increase the activity of methanol synthesis catalysts, the difference in activity when using various supports, and the fact that oxidants increase the reaction rate (CO_2 is hydrogenated at lower temperatures than CO) should be related to stabilisation of cationic gold. The following key questions, therefore, arise:

- What is the likely catalytic mechanism of methanol synthesis over the recently found gold catalysts, and is the mechanism similar/different to that over copper catalysts?
- How does interaction of a gold cluster with an oxidant affect the cluster's electronic density?
- What role will the support in Au/MeO catalysts play?

Many of the concepts involved in heterogeneous catalysis, e.g. active catalyst centres and stable reaction intermediates, are difficult to determine experimentally. Molecular modelling has the potential to predict properties of catalysts that have not been synthesized, sometimes eliminating the need for expensive experiments (Broadbelt and Snurr, 2000). In particular, quantum mechanical results, which are solutions to the Schrödinger equation, can be used to predict molecular properties like geometries, energetics, and distribution of electron density in molecules. Information obtained can be used as a guide in selecting appropriate experiments and designing more selective catalysts.

The aim of this project was, therefore, to perform ab initio studies on gold catalysed methanol synthesis, in order to investigate the mechanistic aspects of this reaction over gold catalysts. Parallel calculations with copper and zinc were also performed, in order to determine any fundamental differences/similarities between the Au/ZnO and the Cu/ZnO catalyst systems.

To further investigate possible support effects in Au/ZnO catalysts, calculations on gold and zinc-modified gold clusters were performed. The objective was to investigate the effect of cluster modification on the distribution of electron density in the cluster.

2 BASIC PRINCIPLES OF AB INITIO QUANTUM CHEMISTRY[1]

2.1 The Schrödinger Equation

Ab initio quantum chemistry is concerned with solving chemical problems by finding solutions to the Schrödinger equation:

$$H\psi = E\psi \qquad (2.1)$$

H is a Hamiltonian, an energy operator on ψ. E is the numerical value of the energy of the system under consideration. ψ is a wavefunction for the particles. Its value depends on the position of the particles, and, in the case of electrons, on their spin. It should be emphasized that a wavefunction is just a mathematical function that describes the location and motion of the particles.

For a given particle, the Born interpretation of a wavefunction is that the quantity, $\psi.\psi^*$, at a particular point represents the probability of finding an electron at that point. Integration of $\psi.\psi^*$ over all space, thus, equals unity.

The significance of the Schrödinger equation (2.1) is that the energy of a system can be computed once the wavefunction is known. The energy, or its expectation value (as is commonly called), is calculated in this manner:

$$E = \int \psi^* H \psi d\tau \qquad (2.2)$$

where $d\tau$ indicates that the integration is over all space. The only problem in an ab initio calculation is, therefore, to find the wavefunction that describes the system of interest. This is not a trivial task, and consequently, the Schrödinger equation can be solved exactly only for the hydrogen atom and the simplest molecular species, H_2^+.

[1] The material presented in this section was adapted from the following references: Henre *et al.*, 1986; Atkins, 1994; Russo *et al.*, 1995; Bond, 2000 and Leach, 2001.

2.2 Separation of Nuclear and Electronic Motions

The velocities of the electrons are much higher than the velocities of the nuclei, and the nuclei are much heavier than the electrons. It is, thus, reasonable to expect that the electrons can instantaneously adjust to any changes in the positions of the nuclei. To simplify calculations for molecular systems (usually with many nuclei and electrons), one can assume that the nuclei are fixed in position, and only the electrons are moving. This approximation is known as the Born-Oppenheimer approximation, and it allows a decoupling of nuclear and electronic motions. The total wavefunction is thus:

$$\psi_{tot} = \psi(\text{electrons}) \,.\, \psi(\text{nuclei}) \qquad (2.3)$$

2.3 The Many Body Problem

As stated, the objective in an ab initio calculation is to find a reasonable approximation to the wavefunction of the molecular system of interest, from which the electronic structure can be deduced. The most common ab initio technique for the treatment of molecular systems is the molecular orbital method. In this method, one-electron wavefunctions, or orbitals, are used to approximate the full wavefunction. A maximum of two electrons, with opposite spins, are allowed in a single molecular orbital. This is the basis of the Hartree-Fock (HF) method for a closed-shell system. Each molecular orbital can further be described as linear combination of basis functions (ϕ_μ) , which are typically centred around the atoms in the molecule:

$$\psi_i = \sum_{\mu=1}^{n} C_{\mu i}\phi_\mu \qquad (2.4)$$

The molecular orbital expansion coefficients, $C_{\mu i}$, will be adjusted to give the most satisfactory molecular orbitals for the molecular system of interest. In the Unrestricted Hartree-Fock (UHF) method, the molecular orbitals are not restricted to be doubly occupied. This means that electrons with opposite spins that occupied the same orbital in the closed-shell system can now have different molecular orbital expansion

coefficients, $C_{\mu i}$. The chemical problem has now been reduced to finding the appropriate basis functions (or basis sets) for the system of interest.

2.4 Basis Sets

The basis sets employed in most ab initio calculations are made up of atomic orbitals. Slater-type orbitals (STOs), also known as hydrogen-like orbitals, were found to be adequate for the describtion of a hydrogen atom. An example of a 1s orbital is given below:

$$\phi_{1s} = (\frac{\zeta^3}{\pi})^{1/2} \exp(-\zeta r) \tag{2.5}$$

where ζ is a constant that determines the size of the orbital, and r is the position in space. Similar forms exist for the 2s and 2p orbitals.

Using the Slater-type orbitals (STOs) in molecular systems turned out to be difficult, due to the fact that some of the integrals become almost impossible to evaluate, especially when orbitals are centered around different nuclei. Consequently, the Slater orbitals are frequently replaced by Gaussian functions, or Gaussian-type orbitals (GTOs). These are the powers of x,y and z, multiplied by $\exp(\alpha r^2)$, with α determining the radial extent (or spread) of the function. The smaller the value of α, the larger the spread. The first four Gaussians are shown below:

$$g_s = (\frac{2\alpha}{\pi})^{3/4} \exp(-\alpha r^2) \tag{2.6}$$

$$g_x = (\frac{128\alpha^5}{\pi^3})^{1/4} x \exp(-\alpha r^2) \tag{2.7}$$

$$g_y = (\frac{128\alpha^5}{\pi^3})^{1/4} y \exp(-\alpha r^2) \tag{2.8}$$

$$g_z = (\frac{128\alpha^5}{\pi^3})^{1/4} z \exp(-\alpha r^2) \tag{2.9}$$

The first Gaussian has an s-orbital angular symmetry, while the other three Gaussians have p-orbital symmetry. The variables x, y, z are the coordinates of the centres of the Guassians.

Integrals in Gaussian functions can be evaluated explicitly without recourse to numerical integration, making them more attractive than Slater-type orbitals.

A *minimal basis* set contains the minimum number of functions required to accommodate all the filled orbitals in an atom. STO-nG basis sets are minimal basis sets in which n Gaussian functions are used to represent each orbital. The radial exponents of the Gaussians are not allowed to vary in size during a calculation. This implies that Gaussians of the same size are used on atoms of different sizes (in particular, with different numbers of electrons). It thus, does not come as a surprise that the *minimal basis* sets are inaccurate for compounds containing atoms at the end of a period, e.g oxygen and fluorine. More than one function can, however, be used for each orbital to alleviate this deficiency. A *double zeta* basis set doubles the number of functions in the *minimal basis* set. Such a basis set can partly describe the non-spherical anisotropic aspects of molecular charge distributions.

Core orbitals, unlike valence orbitals, do not affect bonding in a molecule. Therefore, a minimum number of basis functions can be retained for the core orbitals, and only doubled for the valence orbitals. Such basis sets are known as the *split-valence* double zeta basis sets. An example of such a basis set is the 3-21G basis set, where three Gaussians are used to represent the core orbitals. The valence orbitals are also represented by three Guassians: two for the 'contracted' part and one for the 'diffuse' part.

To fully describe the non-spherical anisotropic aspects of molecular charge distributions, *polarisation* functions should be introduced into the basis set. These are functions of higher angular quantum number (e.g p-orbital for hydrogen and d-orbital for first- and second-row elements) that can explain why the charge distribution about an atom in a molecule is changed relative to the isolated atom. A 6-31G basis set with an added polarisation function will be written 6-31G*. The basis sets can further be improved by adding *diffuse* functions, which account for existence of electron density

very far from the nucleus, e.g anions and molecules with lone pairs. The presence of '+' in the basis set description indicates the presence of a diffuse function.

2.5 Electron Correlation Methods

A major disadvantage of the Hartree-Fock method is that it assumes that an electron is moving in an average potential of the other electrons. In reality, the movement of electrons is highly correlated, and they tend to avoid each other. This electron-correlation results in lowering of the total energy. Various methods have been proposed to include correlation effects in ab initio calculations.

2.5.1 Møller-Plesset Pertubation Theory

The Møller-Plesset pertubation theory (MP) is widely used to include correlation effects in calculations. It works on the idea that while the Hartree-Fock solution is an approximate solution to the exact Hamiltonian operator, it is an exact solution for an approximate Hamiltonian operator. The difference between the exact Hamiltonian and the approximate Hamiltonian can be treated as a small pertubation. Any Hamiltonian can be written:

$$H=H_0 +\lambda V \qquad (2.10)$$

where λ varies between 0 and 1: it has a value of 1 for the true Hamiltonian, and 0 for the Hamiltonian corresponding to the Hartree-Fock solution (zeroth-order Hamiltonian). The total electronic wavefunction is expressed in terms of high-order wavefunctions:

$$\psi_i = \psi_i^{(0)} + \lambda \psi_i^{(1)} + \lambda^2\psi_i^{(2)} + \lambda^3\psi_i^{(3)} + \ldots\ldots \qquad (2.11)$$

The pertubation, V, will be solved for in the process of solving for the high-order wavefunctions. An MP2 calculation implies a Møller-Plesset calculation with corrections up to the second-order.

2.5.2 The Variation Method

The variation principle states that all approximate wavefunctions will give expectation values of the energy which are higher than the true energy. The Hartree-Fock wavefunction can be adjusted by adding to it components that represent excited configurations of the wavefunction. These excited configurations can be from promotion of two electrons from occupied orbitals of the Hartree-Fock wave function (Configuration Interaction with double excitation, or CID), or from a combination of single and double excitations (CISD). Within the limitations imposed by a given basis set, this method represents the most complete treatment of electron correlation for a given system. However, this method has very slow convergence.

2.5.3 Density Functional Theory

For treatment of systems containing transition metals, a common method of accounting for electron correlation is to express the total energy as a functional of the electron density, E[ρ(r)]. This method is called Density Functional Theory (DFT). The total energy is written:

$$E[\rho(r)] = \int V_{ext}(r)\rho(r)dr + F[\rho(r)] \qquad (2.12)$$

where the first term represents interaction of electrons with an external potential, and the second term is a density functional that yields the sum of the kinetic energy of the electrons and the contributions from interactions within the electrons themselves. The major differences between various DFT methods in literature are due to the different forms of the functional, F[ρ(r)]. If F[ρ(r)] has a simple dependence on ρ(r), then the DFT method is said to be 'local'. However, if F[ρ(r)] depends on the gradients of ρ(r), then the method is said to be 'gradient-corrected'. Recalling that the square of a wavefunction at a particular point represents the probability of finding an electron there, the electron density, ρ(r), can be written as the sum of the square moduli of a set of one-electron orbitals, i.e:

$$\rho(r) = \sum_{i=1}^{N} |\psi_i(r)|^2 \qquad (2.13)$$

These orbitals are often referred to as the 'Kohn-Sham' orbitals.

2.6 Effective Core Potentials

Heavy elements with 5d, 6s or 6p electrons frequently display unusual chemical and optical properties which can only be explained if relativistic effects are taken into account. Due to the high positive nuclear charge, the orbiting electrons move faster in order to remain in orbit. The inner electrons, most nototably those in the 1s orbital, increase in mass because their speeds approach that of light:

$$m = \frac{m_0}{\sqrt{(1-\frac{v^2}{c^2})}} \tag{2.14}$$

where m is the actual mass of the electron, m_0 is its rest mass, v is the electron's velocity, while c is the speed of light. This scenario results in contraction of the inner orbitals.

Effective core potentials (ECPs) can be used in ab initio calculations to overcome these dominant effects of relativity. An effective potential replaces the inner electrons, which are chemically inert. ECPs can be used in DFT, Hartree-Fock, or MP calculations. An additional advantage of ECPs is that the calculations become faster due to the reduced number of electrons in the system.

3 COMPUTATIONAL APPROACH

3.1 Introduction

It is often difficult to choose an appropriate model system for a theoretical study of phenomena in heterogeneously catalysed reactions. All physical models should converge to principles of quantum physics, which is difficult to apply for an infinite surface. From a chemist's point of view, interaction of a gas molecule with an extended structure is local (Hoffmann, 1988). The use of 1-2 atom clusters to model gas-surface interactions is thus an appropriate starting point for ab initio studies of a reaction mechanism. More metal atoms can be added to the cluster to investigate effects of nearest neighbour interactions on the bonding potential of the interacting site. This was the basic approach followed in selecting model systems for the theoretical investigation of gold-catalysed methanol synthesis.

3.2 Surface Intermediates

Kakumoto (1995) and various other workers (e.g. Jung and Bell, 2000 and Koeppel *et al.*, 1991) identified oxygen bonded intermediates as the key intermediates in methanol synthesis over copper catalysts. In this study, the relative energies of various intermediates bonded on copper, zinc and gold atoms were computed, in order to determine a low energy route and active sites for the formation of methanol over Cu/ZnO and Au/ZnO catalysts. The intermediates considered are shown in Figure 3.1. These are: adsorbed carbon dioxide, adsorbed formaldehyde, formates (mono-and bi-dentate), hydroxymethyl, oxycarbinol (mono- and bi-dentate) and methoxy. In addition to the relative energies of the intermediates on the metal atoms, the distribution of electron density for the equilibrium structures were also of interest. The relative energies were computed as follows:

The overall reaction to an intermediate is:

$$CO_2 + (2+x/2 - y)H_2 + M = M\text{-}CH_xO_y + (2-y)H_2O. \qquad (3.1)$$

The relative energy change is thus:

$$\Delta E = E(M\text{-}CH_xO_y) + (2\text{-}y)\,E(H_2O) - E(CO_2) - (2+x/2-y)E(H_2) - E(M), \quad (3.2)$$

where M = Cu, Au, and Zn atoms or cations.

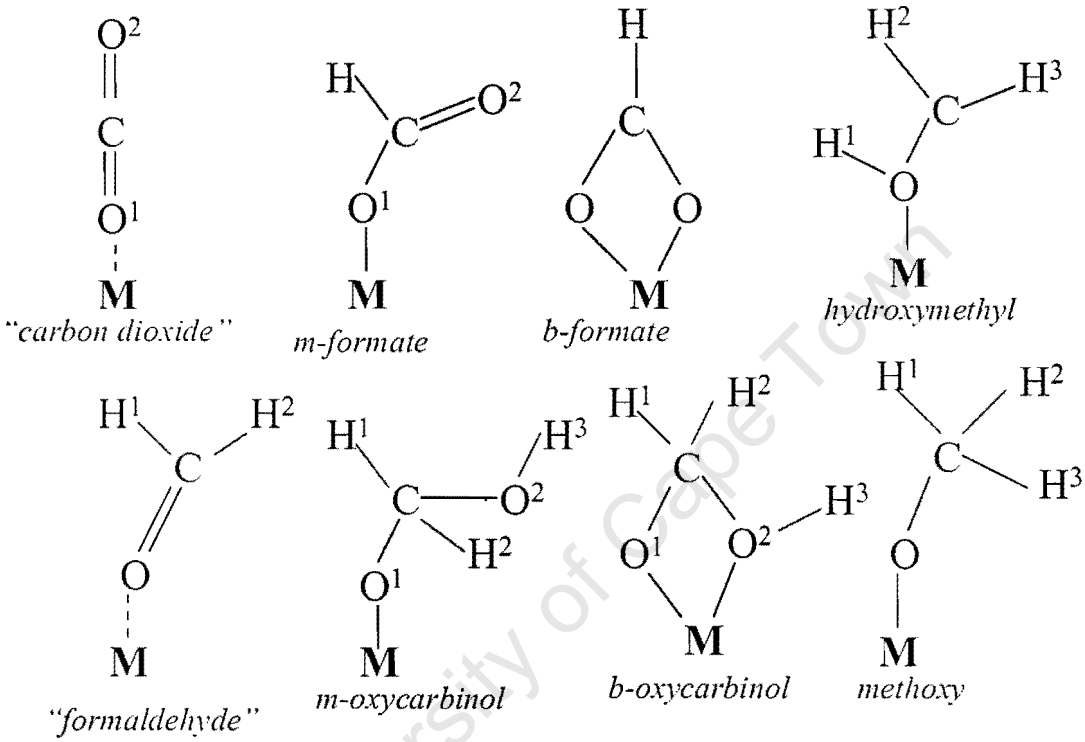

Figure 3.1: Intermediates considered for the study of CO_2 hydrogenation over single metal atoms. M=Cu, Zn, or Au atoms. The numbers differentiate similar atoms in different chemical environments.

3.3 Electronic Effects on an Au (111) Cluster

The distribution of electron density on an Au_7 cluster, representing two adjacent four-fold hollow sites of an Au (111) surface, was calculated to identify an active centre. All atoms were on one plane (see Figure 3.2).

Two oxygen atoms were placed above the Au_7 cluster, forming an Au_7O_2 cluster, to investigate the change in electron density distribution when oxygen atoms enter the surface (see Figure 3.3). The oxygen atoms were placed such that the Au-O-Au bond is 109°, and it is perpendicular to the surface. The angle of 109° was obtained for Cu-O-Cu and Ag-O-Ag bonds in Cu_2O and Ag_2O crystals using a molecular mechanics software (Molecular Simulations Inc, 2000). The software had no reliable parameters for Au.

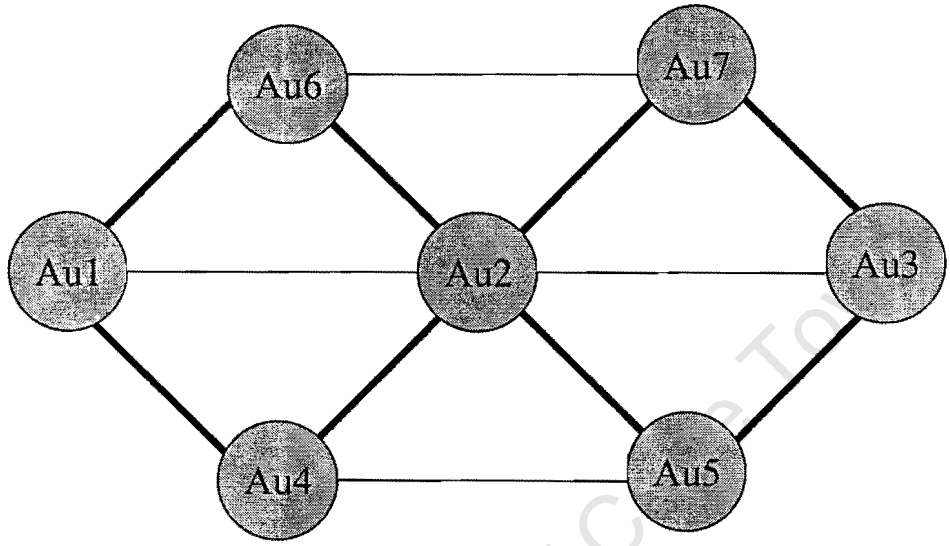

Figure 3.2: A schematic representation of an Au_7 cluster.

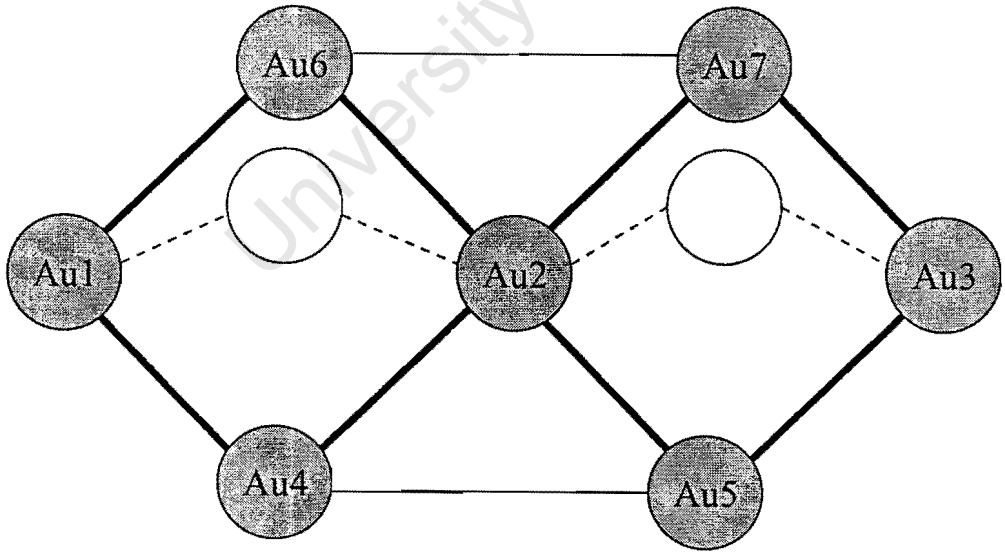

Figure 3.3: A schematic representation of an Au_7O_2 cluster, with oxygen being represented by the hollow circles. The plane of the Au-O-Au bond is perpendicular to the plane of the seven gold atoms.

(a)

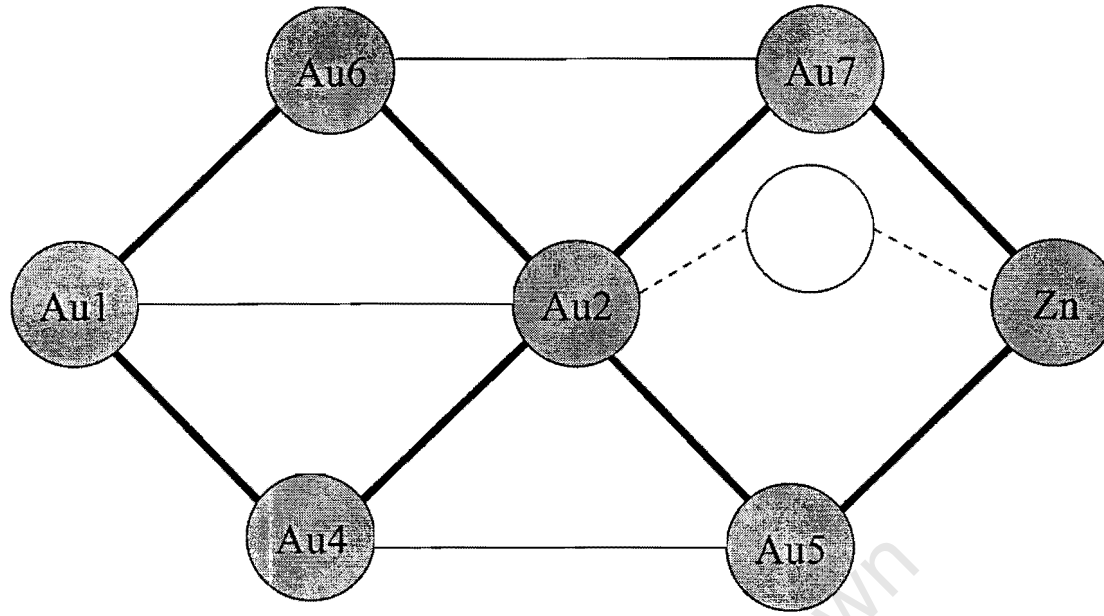

(b)

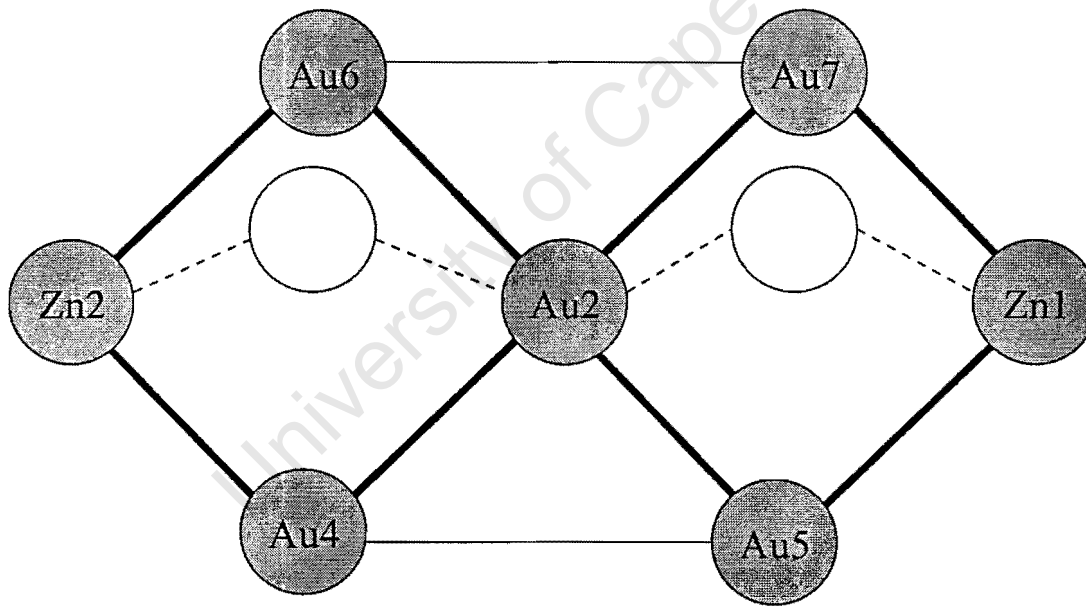

Figure 3.4: Schematic representations of the (a) $Au_6(ZnO)$ and the (b) $Au_5(ZnO)_2$ clusters. Oxygen is represented by the hollow circles.

To investigate the effect of adjacent ZnO entities on the charge distribution of the gold cluster, one (Figure 3.4a) and two (Figure 3.4b) ZnO entities replaced the Au atoms of the Au_7 cluster, to form models of $Au_6(ZnO)$ and $Au_5(ZnO)_2$ surfaces respectively. The distribution of electron density on these clusters was calculated.

It is realised that in an actual Au (111) cluster, the coordination of the central Au atom will be 8, and not 4. The chosen Au_7 cluster is, however, a compromise between molecular and solid state physics, as infinite solids are difficult to model from first principles.

3.4 The Hypothetical "$Au^{\delta+}$-O-Me^{+}" Interface

A simplistic picture of the Au/MeO interface is presented as a linear "$Au^{\delta+}$-O-Me^{+}" entity. Different oxide metals will give different partial charges on the Au atom. In this study, the oxide metal was varied and the distribution of electron density on the interface model was calculated. Three metals were considered: Ti, Fe and Zn. These are the oxide metals for which experimental data on the selectivity of Au/MeO catalysts at the same conversion was available.

3.5 Computation Method

For the study of the reaction mechanisms, the minimum energy structures were obtained at the Unrestricted Hartree-Fock (UHF) level of theory, with no constraints on symmetry. Thermal energy corrections to the total electronic energy, unscaled, were also obtained at the UHF level. The absence of imaginary frequencies confirmed the equilibrium geometries. Energies at the minimum geometry were computed using B3LYP hybrid density functional method proposed by Becke (1993), which includes Hartree-Fock and DFT exchange terms, associated with the gradient-corrected correlation functional by Lee *et al.* (1988). LanL2DZ basis sets by Hay and Wadt (1985) were used for the transition metals. This minimised mass-velocity (relativistic) effects by replacing core electrons with an effective core potential (ECP), and only including the valence electrons in the calculations. For the main group elements, all electrons were included in the calculations using the standard 6-31G basis set. The calculations were carried out using GAMESS quantum mechanical package (Schmidt *et al.*, 1993), on a Unix workstation. Mulliken charges were recorded for the analysis of electron density.

A similar approach was followed for the initial optimisation of the Au_7 cluster. However, the equilibrium geometry of the Au_7 cluster was retained when charge densities in Au_7O_2, $Au_6(ZnO)$ and $Au_5(ZnO)_2$ clusters were computed. In the computations involving the interface model, the GAMESS built-in SBKJC ECP basis sets were used for all the transition metal atoms (Stevens *et al.*, 1992).

The lowest possible spin multiplicity was considered in all cases.

4 RESULTS AND DISCUSSION

4.1 Bonding character of Surface Intermediates

4.1.1 Carbon Dioxide

Table 4.1 shows the bonding character of carbon dioxide on copper, zinc and gold single atoms. The carbon dioxide structure is shown in Figure 4.1. In all cases, carbon dioxide is linearly bonded to the metal atoms, in agreement with a recent theoretical study by Kakumoto (1995) on copper and zinc atoms. The C-O bond for the non-bonded oxygen is about 0.04Å shorter than the bonded side. The metal-oxygen bond length increased in the order Cu < Zn < Au, which implies that carbon dioxide is more strongly bound to copper than zinc. The relative energies of formation of these species were –112, -79, and –84 kJ/mol on Cu, Zn and Au atoms respectively, which did not necessarily correlate with the metal-oxygen bond length. The partial charges on the metal atoms were 0.86, 0.88 and 0.85 for Cu, Zn and Au respectively. The positive partial charges on the metal atoms implies that cationic metal clusters will be required for formation of stable reaction intermediates.

Table 4.1: Relative energies, optimised geometries and atomic charges for carbon dioxide bonded to single metal atoms.

	Cu	Zn	Au
Rel. Energy, kJ/mol	-112	-79	-84
Bond lengths, Å			
R(M-O1)	2.060	2.129	2.377
R(O1-C)	1.181	1.185	1.179
R(C-O2)	1.140	1.137	1.142
Atomic charges, e			
M	+0.86	+0.88	+0.85
O1	-0.41	-0.46	-0.37
C	+0.69	+0.69	+0.67
O2	-0.14	-0.12	-0.15

Figure 4.1: Structure of carbon dioxide coordinated to a metal atom, M.

4.1.2 Formate

The formate species, shown in Figure 4.2, bonds differently on gold than on copper and zinc. The bonding parameters are given on Table 4.2. On copper and zinc atoms, a bi-dentate formate species was obtained, while a mono-dentate species was obtained for the gold atom. The relative energies for this species were –111, -65 and +18 kJ/mol respectively for Cu, Zn and Au atoms. The charges on the metals were 0.43, 1.26 and 0.33 respectively.

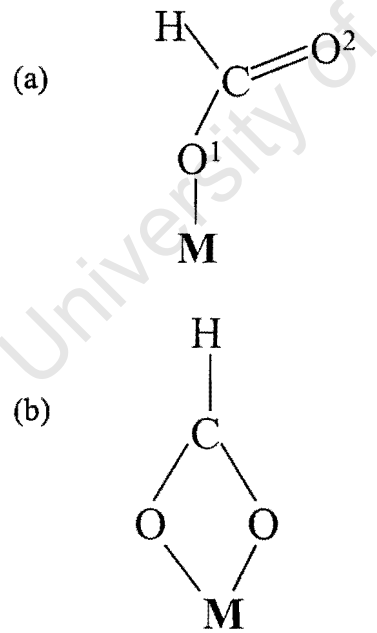

Figure 4.2: Structures of formate species bonded to metal atoms, M, in (a) mono-dentate and (b) bi-dentate modes.

Table 4.2: Relative energies, optimised geometries and atomic charges for formate bonded to single metal atoms.

	Cu	Zn	Au	
Rel. Energy, kJ/mol	-111	-65	+18	
Bond lengths, Å				
R(M-O)	2.139	1.986	R(Au-O)	2.084
R(O-C)	1.268	1.282	R(O1-C)	1.305
R(C-H)	1.078	1.071	R(C-H)	1.082
			R(C-O2)	1.225
Bond and torsion angles, °				
α(O-M-O)	62.3	66.0	α(Au-O1-C)	115.5
α(O-C-H)	119.3	122.3	α(O1-C-H)	113.9
			α(O1-C-O2)	124.7
			δ(Au-O1-C-O2)	0
Atomic charges, e				
M	+0.43	+1.26	Au	+0.33
O	-0.48	-0.50	O1	-0.48
C	+0.37	+0.44	C	+0.37
H	+0.15	+0.30	H	+0.17
			O2	-0.39

4.1.3 Formaldehyde

Figure 4.3 shows the structure of the formate species. This species, which can be formed by hydrogenation of formate, bonds with the M-O-C angle of 180° for Cu and Zn, while the corresponding angle on the Au atom is tilted to 158° (see Table 4.3). There is, thus, an attraction of the $-CH_2$ entity to the surface in the case of the gold atom. The metal-oxygen bond increased in the order Cu < Zn < Au, indicating a weaker binding with the gold surface. The relative energies of the formaldehyde species was –129, -94 and –112 kJ/mol on Cu, Zn and Au atoms respectively. The partial charges on the metals were 0.82, 0.84 and 0.76 on Cu, Zn and Au atoms respectively.

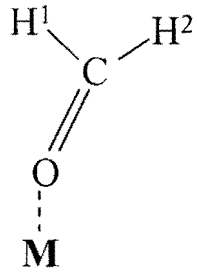

Figure 4.3: Structure of formaldehyde coordinated to a metal atom, M.

Table 4.3: Relative energies, optimised geometries and atomic charges for formaldehyde bonded to single metal atoms.

	Cu	**Zn**	**Au**	
Rel. Energy , kJ/mol	-129	-94	-112	
Bond lengths, Å				
R(M-O)	1.99	2.016	R(Au-O)	2.232
R(O-C)	1.225	1.230	R(O-C)	1.225
R(C-H)	1.077	1.077	R(C-H1)	1.077
			R(C-H2)	1.077
Bond angles, °				
α(M-O-C)	180	180	α(Au-O-C)	157.5
α(O-C-H)	120.7	120.5	α(O-C-H1)	119.9
			α(O-C-H2)	121.2
Atomic charges, e				
M	+0.82	+0.84	Au	+0.76
O	-0.44	-0.48	O	-0.4
C	+0.18	+0.19	C	+0.17
H_1	+0.22	+0.23	H1	+0.24
H_2	+0.22	+0.23	H2	+0.22

4.1.4 Oxycarbinol

Hydrogenation of a formate species can alternatively give an oxycarbinol species, shown in Figure 4.4. Its bonding parameters on Cu, Zn and Au single metal atoms are shown in Table 4.4. The species binds in a bi-dentate fashion to Cu and Zn atoms, while the mono-dentate species is the preferred one on the gold atom. The charges on the metal atoms were 0.40, 0.86 and 0.25 on the Cu, Zn and Au atoms respectively, with the respective relative energies of –59, +7621 and +42 kJ/mol. This result clearly shows that an oxycarbinol species will not form on a zinc surface (see footnote in Table 4.4). On the copper atom, the relative energy of formation of the oxycarbinol species was 70 kJ/mol higher than the relative energy of the formaldehyde species. The relative energy difference between the oxycarbinol and the formaldehyde species over the gold atom was 154 kJ/mol in favour of the formaldehyde species. This result suggests that hydrogenation of the formate species is likely to give a formaldehyde species rather than an oxycarbinol species.

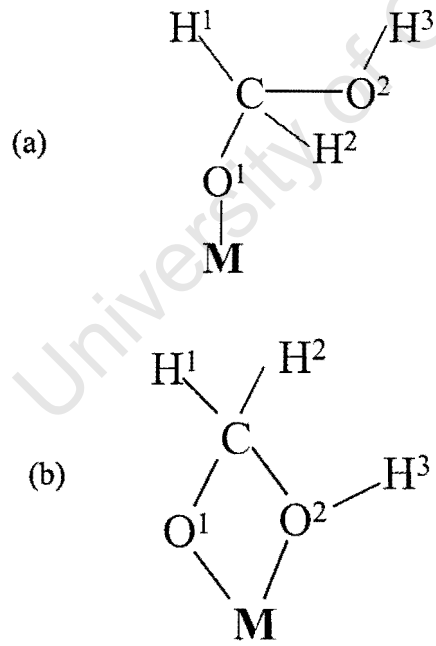

Figure 4.4: Structures of an oxycarbinol species bonded to metal atoms, M, in (a) mono-dentate and (b) bi-dentate modes.

Table 4.4: Relative energies, optimised geometries and atomic charges for oxycarbinol bonded to single metal atoms.

	Cu	**Zn**[1]		**Au**	
Rel. Energy (kJ/mol)	-59	+7612		+42	
Bond lengths, Å					
R(Cu-O1)	1.966	R(Zn-O1)	2.198	R(Au-O1)	2.022
R(Cu-O2)	2.164	R(Zn-O2)	2.197	R(O1-C)	1.393
R(O1-C)	1.352	R(O1-C)	1.392	R(O2-C)	1.431
R(O2-C)	1.521	R(O2-C)	1.392	R(C-H1)	1.084
R(C-H1)	1.085	R(O1-H1)	0.954	R(C-H2)	1.078
R(C-H2)	1.085	R(C-H2)	1.072	R(O2-H3)	0.952
R(O2-H3)	0.952	R(O2-H3)	0.954		
Bond and torsion angles, °					
α(Cu-O1-C)	100.8	α(Zn-O1-C)	100.2	α(Au-O-C)	120.4
α(O1-Cu-O2)	66.8	α(O1-Zn-O2)	58.8	α(O-C-O)	112.7
α(H1-C-H2)	110.3	α(H2-C-O2)	119.2	α(C-O2-H3)	111.8
α(Cu-O2-H3)	155.2	α(Zn-O2-H3)	140.8	α(H1-C-H2)	110.2
δ(Cu-O1-C-H1)	115.5	δ(Zn-O1-C-H2)	135.6	δ(Au-O1-C-O2)	49.1
Atomic charges, e					
Cu	+0.40	Zn	+0.86	Au	+0.25
O1	-0.59	O1	-0.85	O1	-0.54
O2	-0.65	O2	-0.85	O2	-0.58
C	+0.24	C	+0.56	C	+0.18
H1	+0.12	H1	+0.51	H1	+0.16
H2	+0.12	H2	+0.24	H2	+0.16
H3	+0.36	H3	+0.51	H3	+0.37

[1]A 'true' oxycarbinol species did not form on zinc. The stable structure that was obtained had two OH groups, instead of one, and a CH bond. The geometry given is with H1 bonded to O1. It bonded to zinc through two oxygens.

4.1.5 Methoxy

A methoxy species, shown in Figure 4.5, can be formed during hydrogenation of formaldehyde or oxycarbinol species. Over all the metal atoms studied, this species bonds with a tilted M-O-C angle (see Table 4.5). The metal-oxygen bond length increases in the order Zn < Cu < Au. The relative energy of this species over the metal atoms is –52, -21 and +20 kJ/mol on Cu, Zn and Au atoms respectively. The charges on the metals were 0.39, 1.23 and 0.24 on Cu, Zn and Au atoms respectively.

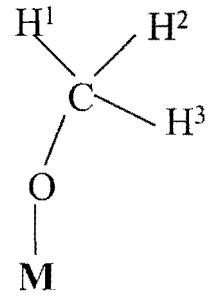

Figure 4.5: Structure of methoxy coordinated to a metal atom, M.

4.1.6 Hydroxymethyl

Another possible product of formaldehyde (or oxycarbinol) hydrogenation is a hydroxymethyl species, shown in Figure 4.6. The bonding parameters of this species on Cu, Zn and Au atoms are shown in Table 4.6. On Cu and Zn atoms, this species had a higher relative energy than the methoxy species, the energy difference between the two species being 15 and 25 kJ/mol over the Cu and Zn atoms respectively. On the Au atom, the relative energy difference between hydroxymethyl and methoxy species was 50 kJ/mol in favour of the hydroxymethyl species. Therefore, formation of this species is energetically more feasible over gold. The partial charges on the metal atoms were all positive.

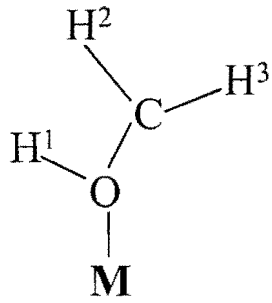

Figure 4.6: Structure of hydroxymethyl coordinated to a metal atom, M.

Table 4.5: Relative energies, optimised geometries and atomic charges for methoxy bonded to single metal atoms.

	Cu	Zn	Au
Rel. Energy, kJ/mol	-52	-21	+20
Bond lengths, Å			
R(M-O)	1.826	1.723	2.001
R(O-C)	1.401	1.443	1.422
R(C-H1)	1.088	1.078	1.080
R(C-H2)	1.091	1.078	1.086
R(C-H3)	1.091	1.080	1.086
Bond and torsion angles, °			
α(M-O-C)	143.8	151.6	123.8
α(H1-C-O)	110.0	108.0	112.4
α(H3-C-H2)	107.5	110.1	108.1
δ(M-O-C-H1)	179.7	117.3	61.3
Atomic charges, e			
M	+0.39	+1.23	+0.24
O	-0.64	-0.70	-0.55
C	-0.10	-0.15	-0.15
H1	+0.13	+0.21	+0.16
H2	+0.11	+0.21	+0.14
H3	+0.11	+0.19	+0.14

Table 4.6: Relative energies, optimised geometries and atomic charges for hydroxymethyl bonded to single metal atoms.

	Cu	Zn	Au
Rel. Energy, kJ/mol	-37	+4	-30
Bond lengths, Å			
R(M-O)	2.016	2.048	2.225
R(O-C)	1.422	1.435	1.422
R(O-H1)	0.953	0.958	0.953
R(C-H2)	1.067	1.069	1.067
R(C-H3)	1.069	1.069	1.069
Bond and torsion angles, °			
α(M-O-C)	126.1	121.8	126.6
α(M-O-H1)	120.0	123.7	118.9
α(H3-C-H2)	123.7	126.1	123.9
δ(Cu-O-C-H2)	159.9	94.1	172.8
Atomic charges, e			
M	+0.79	+0.82	+0.66
O	-0.65	-0.71	-0.6
C	-0.01	-0.01	+0.02
H1	+0.46	+0.46	+0.47
H2	+0.20	+0.23	+0.22
H3	+0.21	+0.23	+0.23

4.2 Proposed Reaction Pathways over Cu/ZnO and Au/ZnO Catalysts

Results on the energetics of various species on metal atoms allows the selection of a mechanistic picture for methanol synthesis from the various possibilities shown in Figure 4.7. Favourable mechanisms over copper, zinc and gold metal atoms, are presented in Figures 4.8, 4.9 and 4.10 respectively. After initial formation of formate species, formaldehyde formation is preferred over formation of oxycarbinol species for all metal atoms studied. The formate species on zinc has a lower relative energy than the formate species on gold, but a higher energy than the formate species on copper. Subsequent hydrogenation of formaldehyde will lead to hydroxymethyl

species over gold, and to methoxy species over zinc and copper atoms. Subsequent hydrogenation of either hydroxymethyl or methoxy species leads to methanol. The relative energies of the intermediates on copper are lower than the energies over zinc. This suggests that copper might be the catalytically active material in a Cu/ZnO catalyst. Relative energies of the intermediates over zinc and gold atoms are comparable, suggesting that zinc might possibly act as a co-catalyst in Au/ZnO catalysts. It is known that the ZnO support can form small amounts of methanol (e.g. Huang *et al.*, 1997 and Le Peltier *et al.*, 1997). Therefore, detailed information on the energetics of the transition state structures over Au and Zn might be helpful in determining the relative resistances in methanol synthesis over these two metals. Should zinc not act as a co-catalyst in the two catalysts, the calculations suggest different mechanisms for methanol formation over Au/ZnO and Cu/ZnO catalysts: a "hydroxymethyl" route over gold and a "methoxy" route over copper.

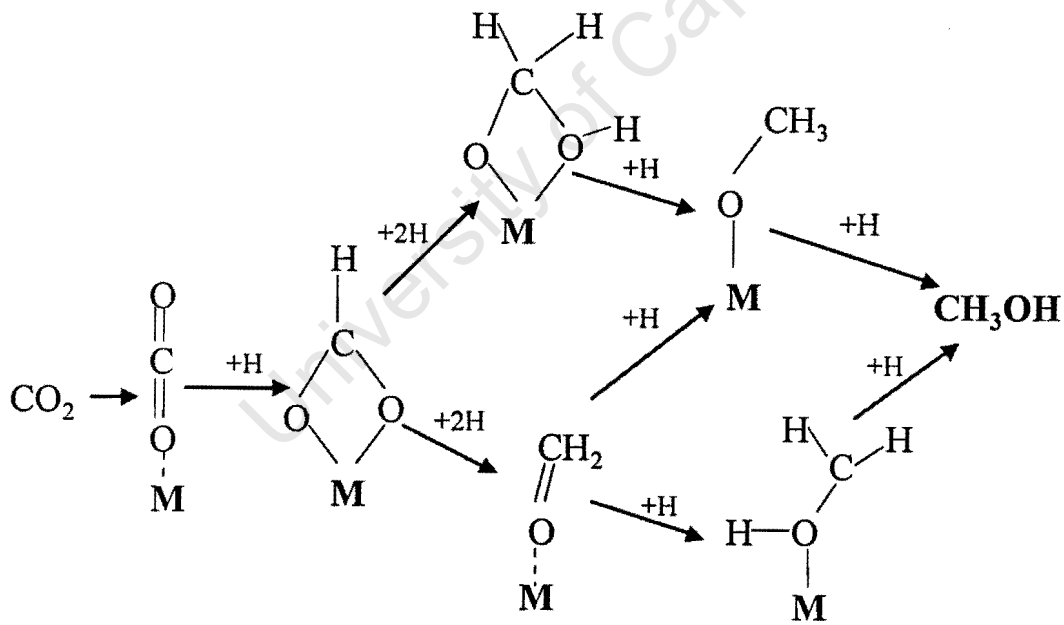

Figure 4.7: Possible mechanisms of methanol synthesis over a metal surface. The formate and oxycarbinol species can also bind in a mono-dentate fashion.

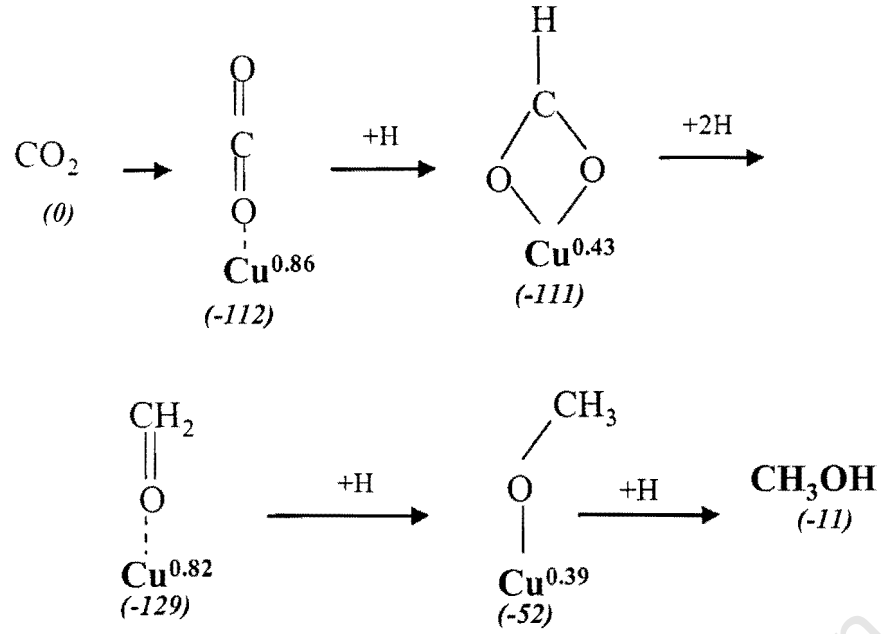

Figure 4.8: A low energy mechanistic pathway of methanol synthesis over a copper atom. Relative energies, in kJ/mol, are shown in parenthesis, while metal charges are shown as superscripts.

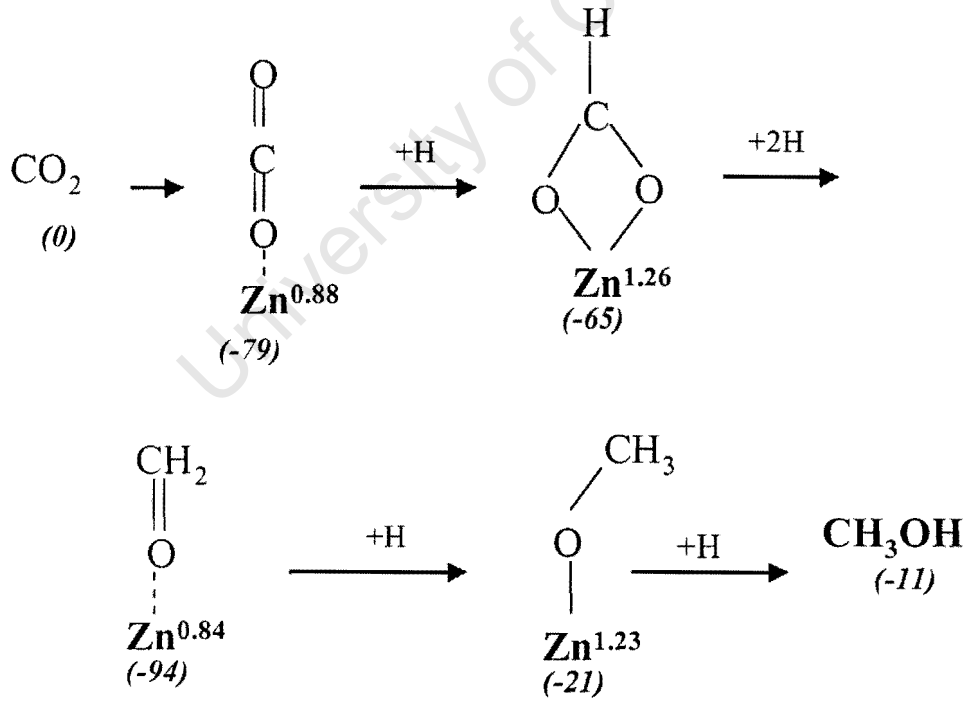

Figure 4.9: A low energy mechanistic pathway of methanol synthesis over a zinc atom. Relative energies, in kJ/mol, are shown in parenthesis, while metal charges are shown as superscripts.

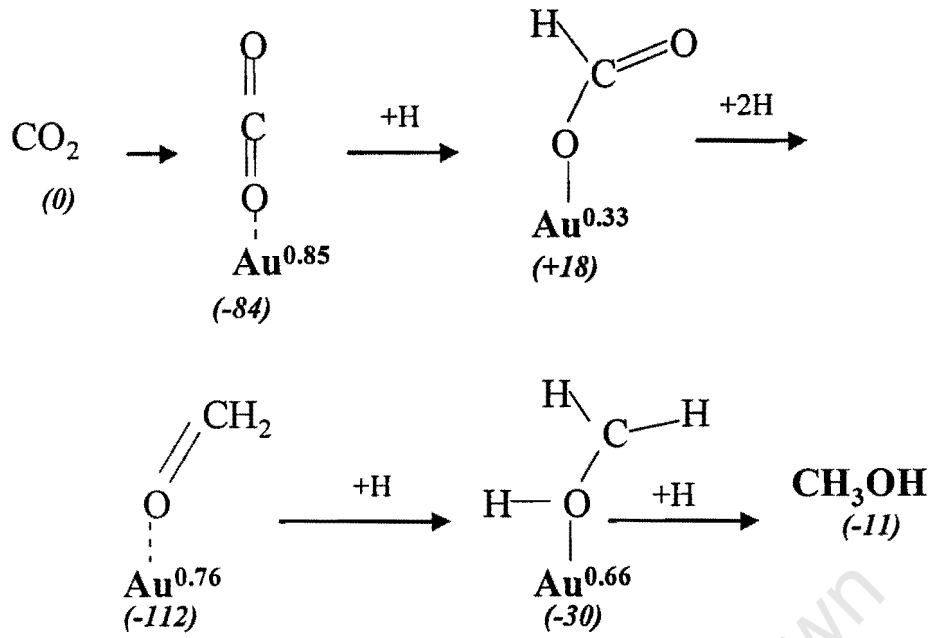

Figure 4.10: A low energy mechanistic pathway of methanol synthesis suggested for a gold atom. Relative energies, in kJ/mol, are shown in parenthesis, while metal charges are shown as superscripts.

4.3 Electronic Properties of Modified Au (111) Surfaces

4.3.1 Bare Au_7 Cluster

Table 4.7 lists the geometrical parameters of an optimised Au_7 (111) cluster, redrawn in Figure 4.11, as well as the distribution of electron density. The Au-Au distance in the cluster varied between 2.79 and 2.97 Å, which was in excellent agreement with the bond distance of 2.883 Å for the Au-Au nearest neighbour distance in the bulk. The peripheral atoms were slightly anionic, or metallic, while the centre atom had a charge of +0.39. This implies that the centre atom is the active site in this arrangement of atoms. Therefore, any factors that increase the effective charge on the centre atom will increase the selectivity of this cluster. Although close enough for all practical purposes, the cluster was slightly unsymmetrical (as evidenced by the charge differences between two identical atoms). As there was no physical reason for this to happen, the result can be attributed to the convergence tolerance used in the calculations. A gradient convergence tolerance value of 0.0001 Hartree/bohr was

used, as it was found to be a good compromise between accuracy and computation time.

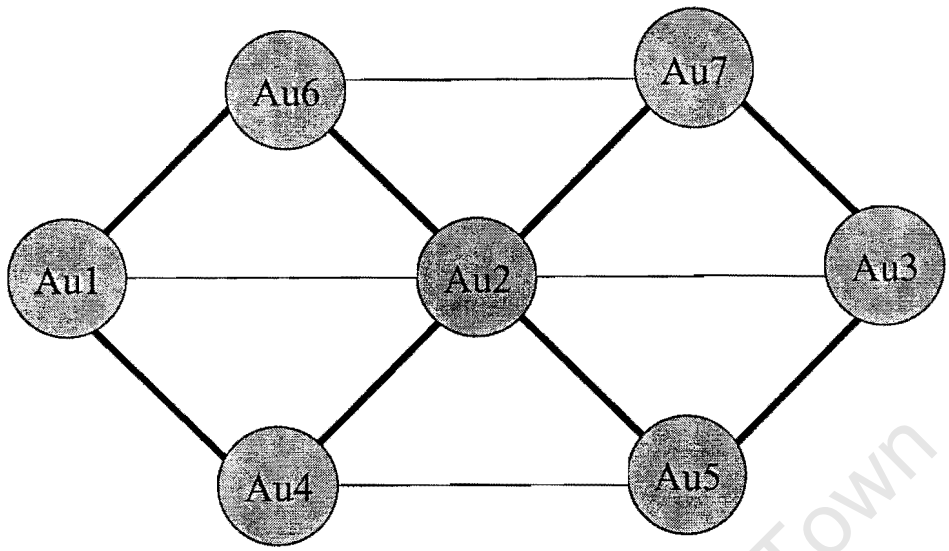

Figure 4.11: A schematic representation of an Au_7 cluster.

4.3.2 Au_7O_2 Cluster

When two oxygen atoms approached the hollow sites of the Au_7 cluster, the charge on the active centre was increased from +0.39 to +0.57(see Table 4.8). The cluster is redrawn in Figure 4.12. Modification of a gold surface with gas phase oxidants should, therefore, increase its catalytic activity for methanol synthesis. Under reaction conditions, the surface concentration of oxygen will depend, amongst other things, on the CO_2/CO ratio of the feed gas. Although bulk gold is chemically inert, oxidation of very small particles should thermodynamically be feasible due to surface energy contributions to the total Gibbs' free energy.

Table 4.7: Charge densities in an optimised structure of the Au_7 cluster.

Atom	**Atomic charge, e**
Au1	-0.13
Au2	+0.39
Au3	-0.13
Au4	-0.03
Au5	-0.04
Au6	-0.04
Au7	-0.02
Atom Pair	**Nearest Neighbour Distances, Å**
Au1-Au4	2.923
Au1-Au6	2.966
Au2-Au6	2.798
Au2-Au4	2.795
Au2-Au7	2.795
Au2-Au5	2.797
Au3-Au7	2.934
Au3-Au5	2.954
Au6-Au7	2.786
Au4-Au5	2.790

4.3.3 $Au_6(ZnO)$ and $Au_5(ZnO)_2$ Clusters

The results for the ZnO modified clusters, redrawn in Figure 4.13, are shown in Tables 4.9 and 4.10. Modifying the Au_7 cluster with one and two units of ZnO increased the partial charge on the active centre from +0.39 to +0.44 and 0.46 respectively. This implies that even in Au/ZnO catalysts, interaction of ZnO with gold particles, probably at the interface, results in stabilisation/increase of the effective charge on the gold particles. This is consistent with the observation that for gold catalysts in general, a large interfacial distance is required for high activity (Haruta, 1997).

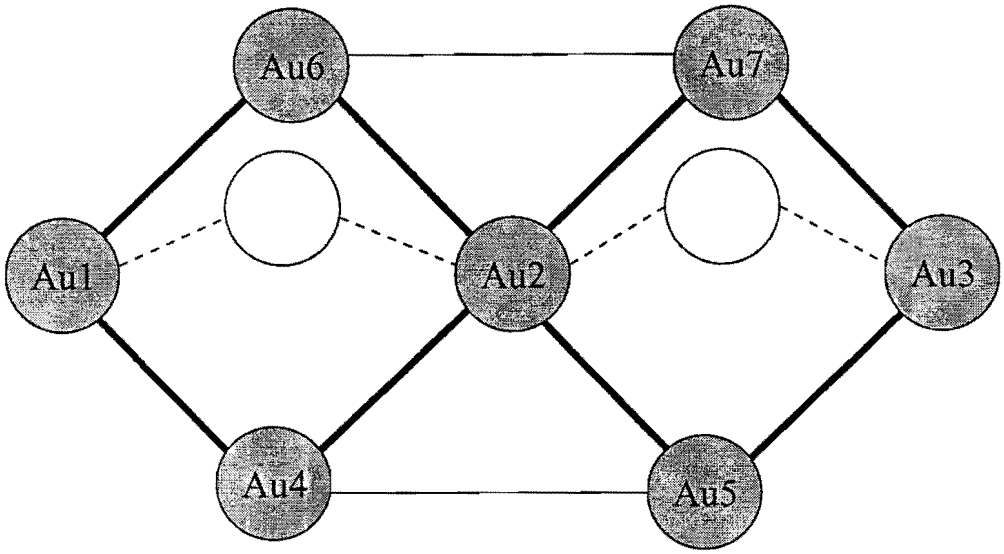

Figure 4.12: A schematic representation of an Au_7O_2 cluster, with oxygen being represented by the hollow circles. The plane of the Au-O-Au bond is perpendicular to the plane of the seven gold atoms.

Table 4.8: Charge densities in an Au_7O_2 cluster.

Atom	Atomic charge, e
Au1	+0.11
Au2	+0.57
Au3	+0.11
Au4	+0.09
Au5	+0.07
Au6	+0.07
Au7	+0.08
O1	-0.56
O2	-0.55

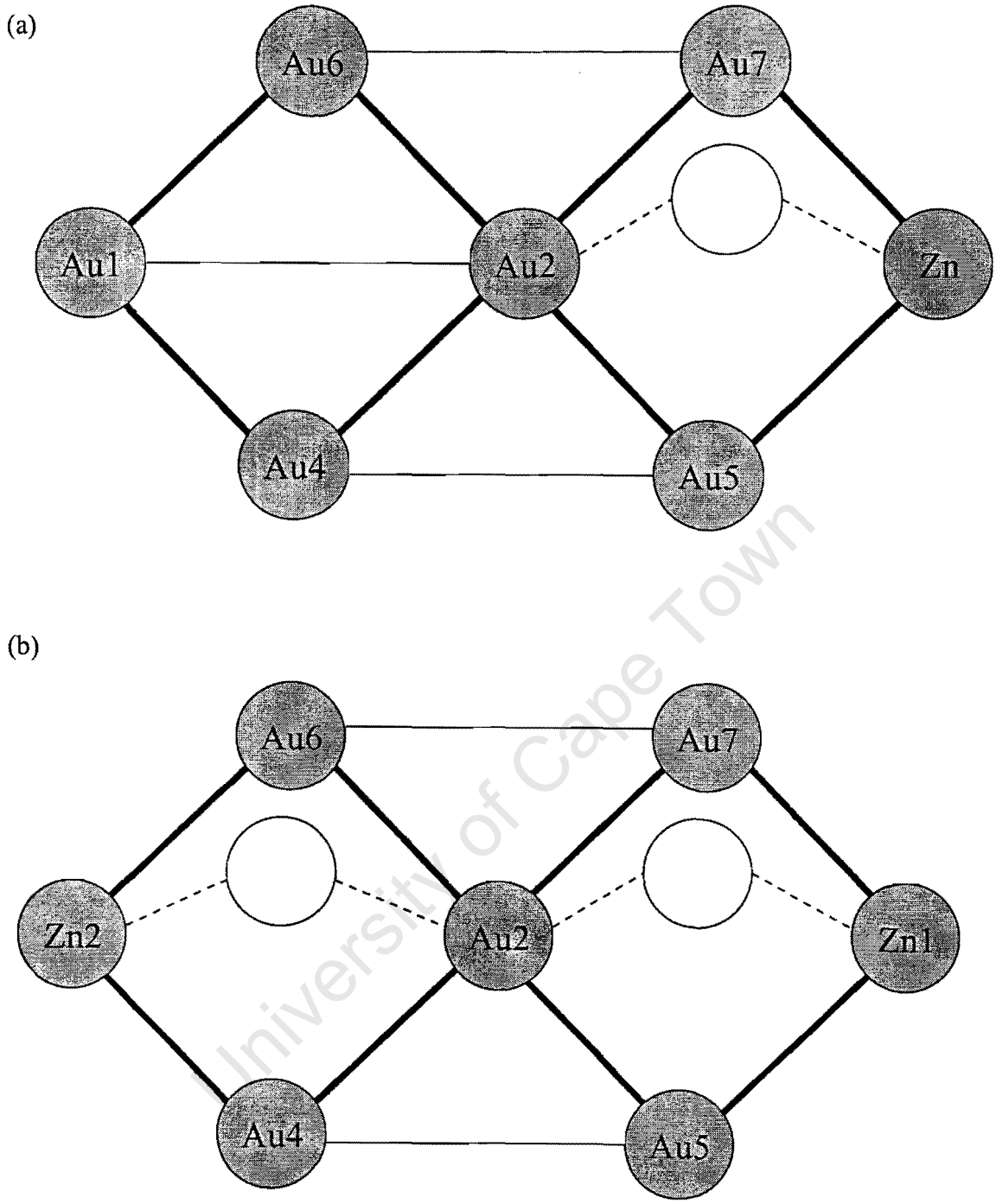

Figure 4.13: Schematic representations of the (a) $Au_6(ZnO)$ and the (b) $Au_5(ZnO)_2$ clusters. Oxygen is represented by the hollow circles.

Table 4.9: Charge densities in an $Au_6(ZnO)$ cluster.

Atom	Atomic charge, e
Au1	-0.12
Au2	+0.44
Zn	+0.76
Au4	-0.09
Au5	-0.11
Au6	-0.10
Au7	-0.11
O1	-0.65

Table 4.10: Charge densities in an $Au_5(ZnO)_2$ cluster.

Atom	Atomic charge, e
Zn2	+0.75
Au2	+0.46
Zn1	+0.76
Au4	-0.19
Au5	-0.18
Au6	-0.18
Au7	-0.19
O1	-0.63
O2	-0.62

4.4 At the Au/MeO Interface: Electronic Effects

Electron density distribution in a simplistic picture of the hypothetical "$Au^{\delta+}$-O-Me^{+}" interface was computed (see Table 4.11), and a correlation was found between the experimental selectivity for methanol synthesis and the partial charge on gold (see Table 4.12). The charge on the gold atom when using various types of oxide metals increased in the order Ti < Fe < Zn, which was the selectivity order obtained experimentally (Sakurai and Haruta, 1995). The experimental results were obtained for gold particles of similar size, clearly showing that the selectivity was not due to

any particle size effects. Although the calculations were performed on a very simplistic picture of the interface, the fact that selectivity correlated very well with the calculated partial charge on gold strongly suggests that the synergy at the Au/MeO interface is due to electronic effects induced by the support.

Table 4.11: Calculated parameters in the Au^{δ}-O^{α}-Me^{β} interface model.

Parameters	Oxide Metal, Me		
	Zn	Fe	Ti
Au-O, Å	2.071	2.073	2.049
O-Me, Å	1.709	1.679	1.763
δ	+0.70	+0.63	+0.59
α	-0.66	-0.56	-0.63
β	+0.95	+0.93	+1.04

Table 4.12: Experimental selectivities for methanol synthesis from CO_2 at similar conversion and particle size (Sakurai and Haruta, 1995)[1].

Catalyst	d_{Au}, nm	Conversion, %	Methanol Selectivity, %
Au/ZnO	3.5	24.5	21.2
Au/Fe_2O_3	3.5	25.3	14.2
Au/TiO_2	3 - 4	25.6	1.2

[1]Reaction conditions: T= 573 K, P=50 atm, GHSV = 3000 ml/hr/g_{cat}, $CO_2/H_2/Ar$ = 23/67/10.

5 CONCLUSIONS

Methanol synthesis over Cu/ZnO catalysts occurs entirely over the copper surface, due to the fact that possible reaction intermediates have higher relative energies on zinc compared to copper. The ZnO support can aid in stabilisation of active Cu^{+} species by forming the Cu^{+}-O-Zn^{n+} interface. However, on Au/ZnO catalysts, bifunctional catalysis can be expected, due to the fact that formation of methanol over a zinc atom is energetically feasible. On gold, a hydroxymethyl species, which has not been reported previously over Cu/ZnO catalysts, was found to have a relative energy which was 50 kJ/mol lower than the energy of the methoxy species. The chemistry of a hydroxymethyl species over gold surfaces should, therefore, be fully investigated in order to establish surface conditions that can increase its stability, and possibly enhance the activity of gold for methanol synthesis.

Formation of stable intermediates on copper, zinc and gold single atoms indicated that cationic species are required for methanol synthesis activity. Therefore, factors that stabilise the charge on the metal atom should increase the activity of the methanol synthesis catalysts.

For an Au (111) surface, cationic centres can be produced/stabilised by letting the surface interact with oxygen, which can be from molecular oxygen or from a gas phase oxygen donor like carbon dioxide. This proposal should be tested experimentally by attempting to regenerate a de-activated gold catalyst via oxidation. Of course, that experiment has a built-in assumption that the mechanism of deactivation is $Au^{+} \rightarrow Au^{0}$ without aggregation to larger particles.

An explanation for the nature of the unspecified synergy at the gold-metal oxide interface is suggested. At the interface, stabilisation of the positive charge on the gold particles occurs as a result of electronic effects induced by the support. Different metal oxides would, therefore, induce dissimilar electronic effects, which is consistent with the observation that different supports result in different selectivity even when the particle size is the same (Sakurai and Haruta, 1995). Selectivity order for supported gold catalysts was predicted using a simple picture of the Au-support

interface, and it agreed with the trend observed experimentally, viz. Au/ZnO > Au/Fe_2O_3 > Au/TiO_2 (Sakurai and Haruta, 1995).

6 REFERENCES

Andreeva, D., Idakiev, V., Tabakova, T., Andreev, A., Giovanoli, R.
Low-Temperature Water-Gas Shift Reaction on Au/α-Fe_2O_3
Applied Catalysis A: General, **134** (1996) 275-283.

Atkins, P.W.
Physical Chemistry
Oxford University Press, United Kingdom, 5th Edition, 1994.

Baiker, A., Kilo, M., Maciejewski, M., Menzi, S., Wokaun, A.
Hydrogenation of CO_2 over Copper, Silver and Gold/Zirconia Catalysts: Comparative Study of Catalyst Properties and Reaction Pathways
Guczi, L., Solymosi, F., Tétényi, P (Editors)
Proceedings of the 10th International Congress on Catalysis
Budapest, 1992.
Studies in Surface Science and Catalysis, **75B** (1993) 1257-1272.

Bamwenda, G.R., Tsubota, S., Nakamura, T., Haruta, M.
The Influence of the Preparation Methods on the Catalytic Activity of Platinum and Gold Supported on TiO_2 for CO Oxidation
Catalysis Letters, **44** (1997) 83-87.

Bart, J.C.J., Sneeden, R.P.A.
Copper-Zinc Oxide-Alumina Methanol Catalysts Revisited
Catalysis Today, **2** (1987) 1-123.

Bartlet, N.
Relativistic Effects and the Chemistry of Gold
Gold Bulletin, **31:1** (1998) 22-25.

Becke, A.D.
Density-Functional Thermochemistry. III. The Role of Exact Exchange
Journal of Chemical Physics, **98:7** (1993) 5648-5652.

Bond, G.C.
The Catalytic Properties of Gold
Gold Bulletin, **5** (1972) 11-13.

Bond, G.C.
Relativistic Phenomena in the Chemistry of the Platinum Group Metals. Effects on Coordination and Chemisorption in Homogeneous and Heterogeneous Catalysis
Platinum Metals Review, **44:4** (2000) 146-155.

Bowler, M., Hadden, R., Houghton, H., Hyland, J.N.K., Waugh, K.C.
The Mechanism of Methanol Synthesis on Copper/Zinc Oxide/Alumina Catalysts
Journal of Catalysis, **109** (1988) 263-273.

Broadbelt, L.J., Snurr, R.Q.
Applications of Molecular Modelling in Heterogeneous Catalysis Research
Applied Catalysis A: General, **200** (2000) 23-46.

Cha, D.Y., Parravano, G.
Surface Reactivity of Supported Gold. 1: Oxygen Transfer Between CO and CO_2
Journal of Catalysis, **18** (1970) 200-211.

Chinchen, G.C., Denny, P.J., Jennings, J.R., Spencer, M.S., Waugh, K.C.
Synthesis of Methanol-Review: Part 1. Catalysts and Kinetics
Applied Catalysis, **36** (1988) 1-65.

Dolan, G.
California Paving the Way for Fuel Cell Vehicles
http://www.methanol.org/fuelcell/press/pr990420.html, 2001.

Duprez, D., Ferhat-Hamida, Z., Bettahar, M.M.
Surface Mobility and Reactivity of Oxygen Species on a Copper-Zinc Catalyst in Methanol Synthesis
Journal of Catalysis, **124** (1990) 1-11.

English, A., Rovner, J., Davies, S.
Methanol
in *Kirk-Othmer Encyclopedia of Chemical Technology*, **16** (1992) 537-556.

Fisher, I.A., Woo, H.C., Bell, A.T.
Effects of Zirconia Promotion on the Activity of Cu/SiO_2 for Methanol Synthesis from CO/H_2 and CO_2/H_2
Catalysis Letters, **44** (1997) 11-17.

Frost, J.C.
Junction Effect Interactions in Methanol Synthesis Catalysts
Nature, **334** (1988) 577-580.

Fujitani, T., Saito, M., Kanai, Y., Kakumoto, T., Watanabe, T., Nakamura, J., Uchijima, T.
The Role of Metal Oxides in Promoting a Copper Catalyst for Methanol Synthesis
Catalysis Letters, **25** (1994) 271-276.

Gomes, J.R.B., Gomes, J.A.N.F., Illas, F.
Methoxy Radical Reaction to Formaldehyde on Clean and Hydroxy Radical-Covered Copper (111) Surfaces: A Density Functional Study
Surface Science, **443** (1999) 165-176.

Gomes, J.R.B. and Gomes, J.A.N.F.
Comparative Study of Geometry and Bonding Character for Methoxy Radical Adsorption on Noble Metals
Journal of Molecular Structure (Theochem), **503** (2000a) 189-200.

Gomes, J.R.B. and Gomes, J.A.N.F.
Adsorption of the Formyl Species on Transition Metal Surfaces
Journal of Electroanalytical Chemistry, **483** (2000b) 180-187

Haruta, M., Yamada, N., Kobayashi, T., Iijima, S.
Gold Catalysts Prepared by Coprecipitation for Low Temperature Oxidation of Hydrogen and Carbon Monoxide
Journal of Catalysis, **115** (1989) 301-309.

Haruta, M., Tsubota, S., Kobayashi, T., Kageyama, H., Genet, M.J.
Low-Temperature Oxidation of CO Over Gold Supported on TiO_2, α-Fe_2O_3, and Co_3O_4
Journal of Catalysis, **144** (1993) 175-192.

Haruta, M.
Size- and Support- Dependency in the Catalysis of Gold
Catalysis Today, **36** (1997) 153-166.

Haruta, M. and Daté, M.
Advances in the Catalysis of Gold Nanoparticles
Applied Catalysis A: General, **222** (2001) 427-437.

Hay, P.J. and Wadt, W.R.
Ab Initio Effective Core Potentials for Molecular Calculations. Potentials for Potassium to Gold Including the Outer Core Orbitals
Journal of Chemical Physics, **82:1** (1985) 299-310.

Hayashi, T., Tanaka, K., Haruta, M.
Selective Vapour-Phase Epoxidation of Propylene over Au/TiO_2 Catalysts in the Presence of Oxygen and Hydrogen
Journal of Catalysis, **178** (1998) 566-575.

Hehre, W.J., Radom, L., Schleyer, P.v.R., Pople, J.A.
Ab Initio Molecular Theory
John Wiley & Sons, Inc, United States of America, 1986.

Herman, R.G., Klier, K., Simmons, G.W., Finn, B.P., Bulko, J.B.
Catalytic Synthesis of Methanol from CO/H_2. I Phase Composition, Electronic Properties, and Activities of the $Cu/ZnO/M_2O_3$ Catalysts
Journal of Catalysis, **56** (1979) 407-429.

Hoffmann, R.
Solids and Surfaces. A Chemist's View of Bonding in Extended Structures
VCH Publisher, Inc., New York, 1988.

Hu, Z., Takahashi, K., Nakatsuji, H.
Mechanism of the Hydrogenation of CO_2 to Methanol on a Cu (100) Surface: Dipped Adcluster Model Study
Surface Science, **442** (1999) 90-106.

Huang, L., Kramer, G.J., Wieldraaijer, W., Brands, D.S., Poels, E.K., Castricum, H.L., Bakker, H.
Methanol Synthesis over Cu/ZnO Catalysts Prepared by Ball Milling
Catalysis Letters, **48** (1997) 55-59.

Iizuka, Y., Fujiki, H., Yamauchi, N., Chijiiwa, T., Arai, S., Tsubota, S., Haruta, M.
Adsorption of CO on Gold Supported on TiO_2
Catalysis Today, **36** (1997) 115-123.

Jung, K. and Bell, A.T.
Role of Hydrogen Spillover in Methanol Synthesis over Cu/ZrO_2
Journal of Catalysis, **193** (2000) 207-223.

Kakumoto, T.
A Theoretical Study for the CO_2 Hydrogenation Mechanism on Cu/ZnO Catalyst
Energy Conversion and Management, **36** (1995) 661-664.

Kakumoto, T. and Watanabe, T.
A Theoretical Study for Methanol Synthesis by CO_2 Hydrogenation
Catalysis Today, **36** (1997) 39-44.

Kanai, Y., Watanabe, T., Fujitani, T., Saito, M., Nakamura, J., Uchijima, T.
Evidence for the Migration of ZnO_x in a Cu/ZnO Methanol Synthesis Catalyst,
Catalysis Letters, **27** (1994) 67-78.

Klier, K., Chatikavanij, V., Herman, R.G., Simmons, G.W.
Catalytic Synthesis of Methanol from CO/H_2
Journal of Catalysis, **74** (1982) 343-360.

Koeppel, R.A., Baiker, A., Schild, C., Wokaun, A.
Carbon Dioxide Hydrogenation over Au/ZrO_2 Catalysts from Amorphous Precusors: Catalytic Reaction Mechanism
Journal of the Chemical Society: Faraday Transactions, **87:17** (1991) 2821-2828.

Leach, R.
Molecular Modelling. Principles and Applications
Pearson Education Limited, England, 2nd Edition, 2001.

Lee, C., Yang, W., Parr, R.G.
Development of the Colle-Salvetti Correlation-Energy Formula into a Functional of the Electron Density
Physical Reviews B: Condensed Matter, **37:2** (1980) 785-789.

Le Peltier, F., Chaumette, P., Saussey, J., Bettahar, M.M., Lavalley, J.C.
In-Situ FT-IR Spectroscopy and Kinetic Study of Methanol Synthesis from CO/H_2 over $ZnAl_2O_4$ and Cu-$ZnAl_2O_4$ Catalysts
Journal of Molecular Catalysis A: Chemical, **122** (1997) 131-139.

Liu, G., Willcox, D., Garland, M., Kung, H.
The Rate of Methanol Production on a Copper-Zinc Oxide Catalyst: The Dependence on the Feed Composition
Journal of Catalysis, **90** (1984) 139-146.

Liu, G., Willcox, D., Garland, M., Kung, H.H.
The Role of CO_2 in Methanol Synthesis on Cu-Zn Oxide: An Isoptope Labelling Study
Journal of Catalysis, **96** (1985) 251-260.

Molecular Simulations Inc.
Materials Studio™ Version 1.1, 2000.

Nakamura, J., Nakamura, I., Uchijima, T., Kanai, Y., Watanabe, T., Saito, M., Fujitani, T.
Methanol Synthesis over a Zn-deposited Copper Model Catalyst
Catalysis Letters, **31** (1995) 325-331.

Okumura, M., Nakamura, S., Tsubota, S., Nakamura, T., Azuma, M., Haruta, M.
Chemical Vapor Deposition of Gold on Al_2O_3, SiO_2, and TiO_2 for the Oxidation of CO and of H_2
Catalysis Letters, **51** (1998) 53-58.

Okumura, M., Kitagawa, Y., Haruta, M., Yamaguchi, K.
DFT Studies of Interaction Between O_2 and Au Clusters. The Role of Anionic Surface Au Atoms on Au Clusters for Catalysed Oxygenation
Chemical Physics Letters, **346** (2001) 163-168.

Ramaroson, E., Kieffer, R., Kiennemann, A.
Reactions of Carbon Dioxide and Hydrogen on Supported Palladium Catalysts
Journal of the Chemical Society, Chemical Communications, **12** (1982) 645-646.

Russo, T.V., Richard, L.M., Hay, P.J.
Effective Core Potentials for DFT Calculations
Los Alamos National Laboratory, *http://www.t12.lanl.gov/~russo/ecp.html, 1995.*

Sahibzada, M., Metcalfe, I.S., Chadwick, D.
Methanol Synthesis from $CO/CO_2/H_2$ over $Cu/ZnO/Al_2O_3$ at Differential and Finite Conversions
Journal of Catalysis, **174** (1998) 111-118.

Sakurai, H., Tsubota, S., Haruta, M.
Hydrogenation of CO_2 over Gold Supported on Metal Oxides,
Applied Catalysis A: General, **102** (1993) 125-136.

Sakurai, H. and Haruta., M.
Carbon Dioxide and Carbon Monoxide Hydrogenation over Gold Supported on Titanium, Iron, and Zinc Oxides
Applied Catalysis A: General, **127** (1995) 93-105.

Sakurai, H. and Haruta, M.
Synergism in Methanol Synthesis from Carbon Dioxide over Gold Catalysts Supported on Metal Oxides
Catalysis Today, **29** (1996) 361-365.

Sandler, S.I.
Chemical and Engineering Thermodynamics
John Wiley and Sons, Inc.
New York, 3^{dr} Edition, 1999.

Schmidt, M.W., Baldridge, K.K., Boatz, J.A., Elbert, S.T., Gordon, M.S., Jensen, J.H., Koseki, S., Matsunaga, N., Nguyen, K.A., Su, J.S., Windus, T.L., Dupuis, M., Montgomery, J.A.
General Atomic and Molecular Electronic Structure System
Journal of Computational Chemistry, **14** (1993) 1347-1363.

Schwank, J.
Applications of Elemental Gold in Heterogeneous Catalysis
Gold Bulletin, **16:4** (1983) 103-110.

Shaw, E.A., Walker, A.P., Rayment, T., Lambert, R.M.
Methanol Synthesis Activity of Au/CeO_2 Catalysts Derived from a $CeAu_2$ Alloy Precursor: Do Schottky Barriers Matter?
Journal of Catalysis, **134** (1992) 747-750.

Solomon, E.
Overseas Business Report (South Africa) - *OBR9209*
University of Missouri, 1992.

Stevens, W.J., Krauss, M., Basch, H., Jasien, P.G.
Relativistic Compact Effective Potentials and Efficient, Shared-Exponent Basis Sets for Third- , Fourth- , and Fifth-Row Atoms
Canadian Journal of Chemistry, **70:2** (1992) 612-630.

Stobinski, L.
Molecular and Atomic Deuterium Chemisorption on Thin Gold Films at 78K: An Isotope Effect
Applied Surface Science, **103** (1996) 503-508.

Stobinski, L., Nowakowski, R., Dus, R.
Atomic Hydrogen Adsorption on Thin Discontinuous and Continuous Gold Films – Similarities and Differences
Vacuum, **48:3-4** (1997) 203-207.

Strømsnes, H., Jusuf, S., Schimmelpfennig, B., Wahlgren, U., Gropen, O.
A Theoretical Study of the Chemisorption of Molecular Hydrogen on a Seven Atom Gold Cluster
Journal of Molecular Structure, **567-568** (2001) 137-143.

Sun, Q., Liu, C., Pan, W., Zhu, Q., Deng, J.
In Situ IR Studies on the Mechanism of Methanol Synthesis over an Ultrafine $Cu/ZnO/Al_2O_3$ Catalyst
Applied Catalysis A: General, **171** (1998) 301-308.

Takagawa, M. and Ohsugi, M.
Study on Reaction Rates for Methanol Synthesis from Carbon Monoxide, Carbon Dioxide, and Hydrogen
Journal of Catalysis, **107** (1987) 161-172.

Ueda, A. and Haruta, M.
Nitric Oxide Reduction with Hydrogen, Carbon Monoxide, and Hydrocarbons over Gold Catalysts
Gold Bulletin, **32:1**(1999) 3-11.

Waters, R.D., Weimer, J.J., Smith, J.E.
An Investigation of the Activity of Coprecipitated Gold Catalysts for Methane Oxidation
Catalysis Letters, **30** (1995) 181-188.

Weirauch, W.
Asia Methanol Demand Growing: Both Capacity, Imports to Rise
http://www.hydrocarbonprocessing.com/archive/archive_98-01/98_01_impact.html.,
1998.

Zhang, Y., Sun, Q., Deng, J., Wu, D., Chen, S.
A High Activity $Cu/ZnO/Al_2O_3$ Catalyst for Methanol Synthesis: Preparation and Catalytic Properties
Applied Catalysis A: General, **158** (1997) 105-120.

APPENDIX A

A1: Poster Presented at a Conference

Phala, N.S., Van Steen, E., Fletcher, J.C.Q., Klatt, G., Koch, K.

Molecular Modeling of Methanol Synthesis Over Au/ZnO catalysts

Catalysis Society of South Africa (CATSA) Conference, Pilanesburg, South Africa, November 2001, *Won a prize for best poster*

A2: An Illustrative GAMESS Calculation

Calculation of the formaldehyde single point energy at the Hartree-Fock optimized geometry

Input File:

```
$CONTRL RUNTYP=ENERGY MAXIT=100 SCFTYP=UHF ICHARG=1 MULT=1 ECP=READ $END
$DFT DFTTYP=B3LYP $END
 $SCF DAMP=.T. $END
 $DATA
Gold
C1
Au 79.0  -1.2988846919  -0.4963767305
 S  3
  1      2.809000000       -1.202155600
  2      1.595000000        1.674157800
  3     0.5327000000       0.3526593000
 S  4
  1      2.809000000        1.160848100
  2      1.595000000       -1.864284600
  3     0.5327000000       -1.035623000
  4     0.2826000000        1.306439900
 S  1
  1     0.5980000000E-01     1.000000000
 P  3
  1      3.684000000      -0.2802681000
  2      1.666000000       0.7818398000
  3     0.5989000000       0.4804776000
 P  2
  1     0.6838000000     -0.9520780000E-01
  2     0.9770000000E-01     1.029914700
 P  1
  1     0.2790000000E-01     1.000000000
 D  2
  1      1.287000000       0.5844273000
  2     0.4335000000       0.5298161000
 D  1
  1     0.1396000000        1.000000000

OXYGEN 8.0 0.9313531605  -0.3971659480
 N31 6

CARBON 6.0 2.0833852286  -0.8148676069
  N31 6

Hydrogen 1.0 2.9066627706  -0.1208865675
   N31 6

Hydrogen 1.0 2.2977883807  -1.8707031470
 N31 6

$END
```

```
$ECP
 AU-ECP GEN 60   4
 5     ----- g potential     -----
    -60.00000000  1     622.62879560
   -555.52923120  2     136.28436070
   -168.00197850  2      33.15497810
    -63.03998750  2       9.98948950
     -4.25166810  2       3.04813120
 6     ----- s-g potential   -----
      3.00000000  0     194.73743040
     38.60208800  1     351.53274470
    864.83707270  2     122.32704020
    374.99355200  2      32.09146170
    289.79101000  2       5.24518120
   -152.45327730  2       4.49162230
 4     ----- p-g potential   -----
      2.00000000  0     420.61588010
     73.88856250  1     109.44178150
    326.67298720  2      34.17142800
    126.58145910  2       5.98797500
 5     ----- d-g potential   -----
3.00000000  0     219.26661580
     55.67931490  1     122.72977860
    449.19873350  2      63.10633690
    215.02690910  2      18.36845200
     64.08409950  2       4.49728440
 5     ----- f-g potential   -----
      4.00000000  0     108.55060370
     51.80653350  1      56.47955270
    231.21831130  2      29.20691590
    119.00473860  2       9.54405430
     15.34241880  2       2.89651180
 O-ECP NONE
 C-ECP NONE
 H-ECP NONE
 H-ECP NONE

 $END
```

Summarised Output File:

```
GRID-BASED DFT OPTIONS
   ---------------
   DFTTYP=B3LYP      QOP  =  0.000   PFTYP =NONE
   NRAD =    96   NTHE =    12   NPHI =    24
   NRAD0 =    24   NTHE0 =     8   NPHI0 =    16


   RUN TITLE
   ---------
Gold

THE POINT GROUP OF THE MOLECULE IS C1
THE ORDER OF THE PRINCIPAL AXIS IS    0

           A TOM          ATOMIC  COORDINATES (BOHR)
          CHARGE          X              Y              Z
AU          79.0    -2.4545361573   -0.9380160073   0.0000000000
OXYGEN       8.0     1.7600022711   -0.7505348134   0.0000000000
CARBON       6.0     3.9370272089   -1.5398764933   0.0000000000
HYDROGEN     1.0     5.4927961751   -0.2284424882   0.0000000000
HYDROGEN     1.0     4.3421904173   -3.5351163522   0.0000000000

      INTERNUCLEAR DISTANCES (ANGS.)
      ------------------------------

                      AU         OXYGEN      CARBON      HYDROGEN

 1 AU                0.0000000   2.2324434 *  3.3972321   4.2222769
 2 OXYGEN            2.2324434 *  0.0000000   1.2254193 *  1.9945371 *
 3 CARBON            3.3972321   1.2254193 *  0.0000000   1.0767523 *
 4 HYDROGEN          4.2222769   1.9945371 *  1.0767523 *  0.0000000
```

5 HYDROGEN 3.8503026 2.0095913 * 1.0773845 * 1.8527240 *

HYDROGEN

1 AU 3.8503026
2 OXYGEN 2.0095913 *
3 CARBON 1.0773845 *
4 HYDROGEN 1.8527240 *
5 HYDROGEN 0.0000000

* ... LESS THAN 3.000

ATOMIC BASIS SET

THE CONTRACTED PRIMITIVE FUNCTIONS HAVE BEEN UNNORMALIZED
THE CONTRACTED BASIS FUNCTIONS ARE NOW NORMALIZED TO UNITY

SHELL	TYPE	PRIMITIVE	EXPONENT	CONTRACTION COEFFICIENTS	
AU					
1	S	1	2.8090000	-1.202155641947	
1	S	2	1.5950000	1.674157858417	
1	S	3	0.5327000	0.352659312306	
2	S	4	2.8090000	1.160848041734	
2	S	5	1.5950000	-1.864284506426	
2	S	6	0.5327000	-1.035622948019	
2	S	7	0.2826000	1.306439834426	
3	S	8	0.0598000	1.000000000000	
4	P	9	3.6840000	-0.280268081600	
4	P	10	1.6660000	0.781839748672	
4	P	11	0.5989000	0.480477568457	
5	P	12	0.6838000	-0.095207800537	
5	P	13	0.0977000	1.029914705805	
6	P	14	0.0279000	1.000000000000	
7	D	15	1.2870000	0.584427276982	
7	D	16	0.4335000	0.529816079133	
8	D	17	0.1396000	1.000000000000	
OXYGEN					
9	S	18	5484.6716600	0.001831074430	
9	S	19	825.2349460	0.013950172200	
9	S	20	188.0469580	0.068445078098	
9	S	21	52.9645000	0.232714335992	
9	S	22	16.8975704	0.470192897984	
9	S	23	5.7996353	0.358520852987	
10	L	24	15.5396162	-0.110777549525	0.070874268231
10	L	25	3.5999336	-0.148026262701	0.339752839147
10	L	26	1.0137618	1.130767015354	0.727158577316
11	L	27	0.2700058	1.000000000000	1.000000000000
CARBON					
12	S	28	3047.5248800	0.001834737132	
12	S	29	457.3695180	0.014037322813	
12	S	30	103.9486850	0.068842622264	
12	S	31	29.2101553	0.232184443216	
12	S	32	9.2866630	0.467941348435	
12	S	33	3.1639270	0.362311985337	
13	L	34	7.8682723	-0.119332419775	0.068999066591
13	L	35	1.8812885	-0.160854151696	0.316423960957
13	L	36	0.5442493	1.143456437840	0.744308290898

14	L	37	0.1687145	1.000000000000	1.000000000000

HYDROGEN

15	S	38	18.7311370	0.033494604338
15	S	39	2.8253944	0.234726953484
15	S	40	0.6401217	0.813757326146
16	S	41	0.1612778	1.000000000000

HYDROGEN

17	S	42	18.7311370	0.033494604338
17	S	43	2.8253944	0.234726953484
17	S	44	0.6401217	0.813757326146
18	S	45	0.1612778	1.000000000000

TOTAL NUMBER OF BASIS SET SHELLS = 18
NUMBER OF CARTESIAN GAUSSIAN BASIS FUNCTIONS = 46
NUMBER OF ELECTRONS = 94
CHARGE OF MOLECULE = 1
SPIN MULTIPLICITY = 1
NUMBER OF OCCUPIED ORBITALS (ALPHA) = 47
NUMBER OF OCCUPIED ORBITALS (BETA) = 47
TOTAL NUMBER OF ATOMS = 5
THE NUCLEAR REPULSION ENERGY IS 275.5397410734
NOTE THIS RUN IS USING CORE POTENTIALS, AND THE NUMBER OF ELECTRONS,
OCCUPIED ORBITALS, AND NUCLEAR REPULSION ENERGY WILL BE ADJUSTED BELOW
AFTER REMOVAL OF THE CORE CHARGES.

ECP POTENTIALS

PARAMETERS FOR "AU-ECP " ON ATOM 1 WITH ZCORE 60 AND LMAX 4 ARE

FOR L= 4	COEFF	N	ZETA
1	-60.00000	1	622.62880
2	-555.52923	2	136.28436
3	-168.00198	2	33.15498
4	-63.03999	2	9.98949
5	-4.25167	2	3.04813
FOR L= 0	COEFF	N	ZETA
1	3.00000	0	194.73743
2	38.60209	1	351.53274
3	864.83707	2	122.32704
4	374.99355	2	32.09146
5	289.79101	2	5.24518
6	-152.45328	2	4.49162
FOR L= 1	COEFF	N	ZETA
1	2.00000	0	420.61588
2	73.88856	1	109.44178
3	326.67299	2	34.17143
4	126.58146	2	5.98798
FOR L= 2	COEFF	N	ZETA
1	3.00000	0	219.26662
2	55.67931	1	122.72978
3	449.19873	2	63.10634
4	215.02691	2	18.36845
5	64.08410	2	4.49728
FOR L= 3	COEFF	N	ZETA
1	4.00000	0	108.55060
2	51.80653	1	56.47955
3	231.21831	2	29.20692
4	119.00474	2	9.54405
5	15.34242	2	2.89651

THE ECP RUN REMOVES 60 CORE ELECTRONS, AND THE SAME NUMBER OF PROTONS.
NUMBER OF ELECTRONS KEPT IN THE CALCULATION IS = 34
NUMBER OF OCCUPIED ORBITALS (ALPHA) KEPT IS = 17
NUMBER OF OCCUPIED ORBITALS (BETA) KEPT IS = 17
THE ADJUSTED NUCLEAR REPULSION ENERGY= 89.9185440854

THE POINT GROUP IS C1 , NAXIS= 0, ORDER= 1

```
 ----------------------------------------

  DIMENSIONS OF THE SYMMETRY SUBSPACES ARE
          A   =  46

..... DONE SETTING UP THE RUN .....
STEP CPU TIME =    0.10 TOTAL CPU TIME =      0.1 (   0.0 MIN)
TOTAL WALL CLOCK TIME=       0.1 SECONDS, CPU UTILIZATION IS 100.00%

     ********************
     1 ELECTRON INTEGRALS
     ********************
TIME TO DO ORDINARY INTEGRALS=     0.01
TIME TO DO     ECP INTEGRALS=     0.20
..... END OF ONE-ELECTRON INTEGRALS .....
STEP CPU TIME =    0.21 TOTAL CPU TIME =      0.3 (   0.0 MIN)
TOTAL WALL CLOCK TIME=       0.3 SECONDS, CPU UTILIZATION IS 100.00%

     -------------
     GUESS OPTIONS
     -------------
     GUESS =HUCKEL         NORB =     0       NORDER=     0
     MIX  =     F       PRTMO =     F       PUNMO =     F
     TOLZ = 1.0E-08        TOLE = 1.0E-05
     SYMDEN=    F       PURIFY=     F

 INITIAL GUESS ORBITALS GENERATED BY HUCKEL   ROUTINE.
 HUCKEL GUESS REQUIRES    21457 WORDS.

 SYMMETRIES FOR INITIAL GUESS ORBITALS FOLLOW.  ALPHA SET(S).
   17 ORBITALS ARE OCCUPIED (   6 CORE ORBITALS).
    7=A     8=A     9=A     10=A    11=A    12=A    13=A
   14=A    15=A    16=A    17=A    18=A    19=A    20=A
   21=A    22=A    23=A    24=A    25=A    26=A    27=A
17 ORBITALS ARE OCCUPIED (   6 CORE ORBITALS).
    7=A     8=A     9=A     10=A    11=A    12=A    13=A
   14=A    15=A    16=A    17=A    18=A    19=A    20=A
   21=A    22=A    23=A    24=A    25=A    26=A    27=A
..... END OF INITIAL ORBITAL SELECTION .....
STEP CPU TIME =    0.04 TOTAL CPU TIME =      0.4 (   0.0 MIN)
TOTAL WALL CLOCK TIME=       0.4 SECONDS, CPU UTILIZATION IS 100.00%

     --------------------
     2 ELECTRON INTEGRALS
     --------------------

 THE -PK- OPTION IS OFF, THE INTEGRALS ARE NOT IN SUPERMATRIX FORM.
 STORING   15000 INTEGRALS/RECORD ON DISK, USING 12 BYTES/INTEGRAL.
 TWO ELECTRON INTEGRAL EVALUATION REQUIRES   60867 WORDS OF MEMORY.
TOTAL NUMBER OF NONZERO TWO-ELECTRON INTEGRALS =           286996
      20 INTEGRAL RECORDS WERE STORED ON DISK FILE  8.
 ..... END OF TWO-ELECTRON INTEGRALS .....
STEP CPU TIME =    1.18 TOTAL CPU TIME =      1.5 (   0.0 MIN)
TOTAL WALL CLOCK TIME=       1.5 SECONDS, CPU UTILIZATION IS 100.00%

     ---------------------------
       U-B3LYP SCF CALCULATION
     ---------------------------

NUCLEAR ENERGY =       89.9185440854
   MAXIT =100    NPUNCH= 2    MULT= 1
   EXTRAP=T  DAMP=T  SHIFT=F  RSTRCT=F  DIIS=T  SOSCF=F
   DENSITY CONV=  1.00E-05
   MEMORY REQUIRED FOR UHF/ROHF STEP=   222598 WORDS.

 DFT CODE IS SWITCHING FROM 96 12 24 TO THE COARSER GRID 24  8 16

   EXCHANGE FUNCTIONAL  =B88&HFX
   CORRELATION FUNCTIONAL=LYP88&VWN5
   DFT THRESHOLD        =.651E-07
   GRID CHANGE THRESHOLD =.300E-03

 ITER EX  TOTAL ENERGY     E CHANGE      DENSITY CHANGE   DIIS ERROR    VIR. SHIFT     DAMPING
  1    0   -249.176252550      -249.176252550     0.344073702          0.611287763   0.000000000   1.000000000
      * * *  INITIATING DIIS PROCEDURE  * * *
```

2	1	-249.443887931	-0.267635382	0.334059793	0.153258212	0.000000000	1.000000000
3	2	-249.307798387	0.136089544	0.250266795	0.268863985	0.000000000	1.000000000
4	3	-249.491581392	-0.183783004	0.065867760	0.112531556	0.000000000	1.000000000
5	4	-249.505614318	-0.014032926	0.013928759	0.013615804	0.000000000	1.000000000
6	5	-249.506038356	-0.000424038	0.007819308	0.006491038	0.000000000	1.000000000
7	6	-249.506161258	-0.000122903	0.000643370	0.000580452	0.000000000	1.000000000
8	7	-249.506162679	-0.000001421	0.000111837	0.000078469	0.000000000	1.000000000

DFT CODE IS SWITCHING BACK TO THE FINER GRID

*** INITIATING DIIS PROCEDURE ***

9	8	-249.496699642	0.009463037	0.016581895	0.006381671
10	9	-249.496840400	-0.000140758	0.001632727	0.000882394
11	10	249.496841141	-0.000000742	0.000992218	0.001006301
12	11	-249.496842963	-0.000001822	0.000382300	0.000736643
13	12	-249.496843487	-0.000000524	0.000093978	0.000115078
14	13	-249.496843510	-0.000000023	0.000020884	0.000014849
15	14	-249.496843510	-0.000000001	0.000009929	0.000006811
16	15	-249.496843511	0.000000000	0.000000605	0.000000449

DENSITY CONVERGED

FINAL U-B3LYP ENERGY IS -249.4968435106 AFTER 16 ITERATIONS
DFT EXCHANGE + CORRELATION ENERGY = -21.9644673578
TOTAL ELECTRON NUMBER = 33.9999454481

SPIN SZ = 0.000
S-SQUARED = 0.000

ENERGY COMPONENTS

WAVEFUNCTION NORMALIZATION = 1.0000000000
ONE ELECTRON ENERGY = -564.5613912767
TWO ELECTRON ENERGY = 225.1460036808
NUCLEAR REPULSION ENERGY = 89.9185440854

TOTAL ENERGY = -249.4968435106

ELECTRON-ELECTRON POTENTIAL ENERGY = 225.1460036808
NUCLEUS-ELECTRON POTENTIAL ENERGY = -721.7040616544
NUCLEUS-NUCLEUS POTENTIAL ENERGY = 89.9185440854

TOTAL POTENTIAL ENERGY = -406.6395138882
TOTAL KINETIC ENERGY = 157.1426703776
VIRIAL RATIO (V/T) = 2.5877090730

..... PI ENERGY ANALYSIS .....

ENERGY ANALYSIS:
FOCK ENERGY= -98.6577576601
BARE H ENERGY= -564.5613912767
ELECTRONIC ENERGY = -331.6095744684
KINETIC ENERGY= 157.1426703776
N-N REPULSION= 89.9185440854
SIGMA PART(1+2)= -269.0049440083
(K,V1,2)= 138.4251983071 -586.2549287710 178.8247864556
PI PART(1+2)= -62.6046304601
(K,V1,2)= 18.7174720705 -135.4491328834 54.1270303527
SIGMA SKELETON, ERROR= -179.0863999229 0.0000000000
MIXED PART= 0.00000E+00 0.00000E+00 0.00000E+00 0.00000E+00
..... END OF PI ENERGY ANALYSIS .....

MULLIKEN AND LOWDIN POPULATION ANALYSES

MULLIKEN ATOMIC POPULATION IN EACH MOLECULAR ORBITAL

ALPHA ORBITALS

	1	2	3	4	5
	1.000000	1.000000	1.000000	1.000000	1.000000
1	0.000167	0.000030	0.999993	0.999169	0.999987
2	0.998980	-0.000452	0.000018	0.000838	0.000013
3	0.000850	0.999582	-0.000011	-0.000008	-0.000001
4	0.000002	0.000420	0.000000	0.000000	0.000000
5	0.000000	0.000420	0.000000	0.000001	0.000000

	6	7	8	9	10
	1.000000	1.000000	1.000000	1.000000	1.000000
1	0.999975	0.000409	0.020601	0.069190	0.052709
2	0.000028	0.778040	0.257362	0.382374	0.379651
3	-0.000003	0.221757	0.516103	0.377326	0.400954
4	0.000000	-0.000820	0.108981	0.005730	0.159543
5	0.000000	0.000615	0.096952	0.165380	0.007142

	11	12	13	14	15
	1.000000	1.000000	1.000000	1.000000	1.000000
1	0.060351	0.839043	0.941886	0.999463	0.998778
2	0.667123	0.090131	0.024662	0.000377	0.000391
3	0.272526	0.027557	0.033452	0.000053	0.000831
4	0.000000	0.020502	0.000000	0.000042	0.000000
5	0.000000	0.022767	0.000000	0.000066	0.000000

	16	17
	1.000000	1.000000
1	0.918453	0.219154
2	0.059835	0.554286
3	0.013998	0.049355
4	0.000456	0.086803
5	0.007257	0.090401

MULLIKEN ATOMIC POPULATION IN EACH MOLECULAR ORBITAL

BETA ORBITALS

	1	2	3	4	5
	1.000000	1.000000	1.000000	1.000000	1.000000
1	0.000167	0.000030	0.999993	0.999169	0.999987
2	0.998980	-0.000452	0.000018	0.000838	0.000013
3	0.000850	0.999582	-0.000011	-0.000008	-0.000001
4	0.000002	0.000420	0.000000	0.000000	0.000000
5	0.000000	0.000420	0.000000	0.000001	0.000000

	6	7	8	9	10
	1.000000	1.000000	1.000000	1.000000	1.000000
1	0.999975	0.000409	0.020601	0.069190	0.052709
2	0.000028	0.778040	0.257362	0.382374	0.379651
3	-0.000003	0.221757	0.516103	0.377326	0.400954
4	0.000000	-0.000820	0.108981	0.005730	0.159543
5	0.000000	0.000615	0.096952	0.165380	0.007142

	11	12	13	14	15
	1.000000	1.000000	1.000000	1.000000	1.000000
1	0.060351	0.839043	0.941886	0.999463	0.998778
2	0.667123	0.090131	0.024662	0.000377	0.000391
3	0.272526	0.027557	0.033452	0.000053	0.000831
4	0.000000	0.020502	0.000000	0.000042	0.000000
5	0.000000	0.022767	0.000000	0.000066	0.000000

	16	17

	1.000000	1.000000
1	0.918453	0.219154
2	0.059835	0.554286
3	0.013998	0.049355
4	0.000456	0.086803
5	0.007257	0.090401

ATOMIC SPIN POPULATION (ALPHA MINUS BETA)

ATOM	MULL.POP.	LOW.POP.
1 AU	0.000000	0.000000
2 OXYGEN	0.000000	0.000000
3 CARBON	0.000000	0.000000
4 HYDROGEN	0.000000	0.000000
5 HYDROGEN	0.000000	0.000000

********* ALL ELECTRONS ********

----- POPULATIONS IN EACH AO -----

		MULLIKEN	LOWDIN
1	AU 1 S	2.11753	0.82697
2	AU 1 S	0.01314	0.57029
3	AU 1 S	0.13429	0.11823
4	AU 1 X	1.99822	1.97530
5	AU 1 Y	1.99740	1.97594
6	AU 1 Z	1.99735	1.97574
7	AU 1 X	0.05013	0.11786
8	AU 1 Y	0.02017	0.04311
9	AU 1 Z	0.00929	0.03160
10	AU 1 X	0.00276	0.03085
11	AU 1 Y	0.00196	0.00650
12	AU 1 Z	0.00255	0.00673
13	AU 1 XX	1.01968	1.24200
14	AU 1 YY	1.24873	1.41358
15	AU 1 ZZ	1.24973	1.41426
16	AU 1 XY	1.81926	1.75153
17	AU 1 XZ	1.80670	1.73785
18	AU 1 YZ	1.81195	1.74231
19	AU 1 XX	0.05871	0.19947
20	AU 1 YY	0.15863	0.23195
21	AU 1 ZZ	0.15956	0.23395
22	AU 1 XY	0.18682	0.26535
23	AU 1 XZ	0.18619	0.26332
24	AU 1 YZ	0.18798	0.25763
25	O 2 S	1.99717	1.99367
26	O 2 S	0.91721	0.85755
27	O 2 X	0.90993	0.85646
28	O 2 Y	1.15557	1.12166
29	O 2 Z	0.83058	0.78262
30	O 2 S	0.95894	0.65402
31	O 2 X	0.42537	0.54491
32	O 2 Y	0.63876	0.68806
33	O 2 Z	0.55379	0.56850
34	C 3 S	1.99652	1.98777
35	C 3 S	0.76327	0.60149
36	C 3 X	0.74731	0.68828
37	C 3 Y	0.84271	0.74237
38	C 3 Z	0.39983	0.36187
39	C 3 S	0.51241	0.43792
40	C 3 X	0.07026	0.29849
41	C 3 Y	0.28254	0.41217
42	C 3 Z	0.21379	0.27181
43	H 4 S	0.53653	0.50907
44	H 4 S	0.22678	0.33370
45	H 5 S	0.54097	0.51419
46	H 5 S	0.24104	0.34109

----- MULLIKEN ATOMIC OVERLAP POPULATIONS -----
(OFF-DIAGONAL ELEMENTS NEED TO BE MULTIPLIED BY 2)

	1	2	3	4	5
1	18.1448343				

```
 2   0.1095460  7.9795069
 3  -0.0154462  0.3988350  4.7315065
 4   0.0019238 -0.0527518  0.3647166  0.5010234
 5  -0.0021389 -0.0478164  0.3490290 -0.0515965  0.5345274

     TOTAL MULLIKEN AND LOWDIN ATOMIC POPULATIONS

   ATOM          MULL.POP.   CHARGE   LOW.POP.   CHARGE
 1 AU          18.238719  0.761281  18.432331  0.567669
 2 OXYGEN       8.387320 -0.387320   8.067442 -0.067442
 3 CARBON       5.828641  0.171359   5.802176  0.197824
 4 HYDROGEN     0.763316  0.236684   0.842772  0.157228
 5 HYDROGEN     0.782005  0.217995   0.855278  0.144722

     ---------------------------------
     BOND ORDER AND VALENCE ANALYSIS    BOND ORDER THRESHOLD=0.050
     ---------------------------------

ATOM PAIR DIST  ORDER     ATOM PAIR DIST  ORDER     ATOM PAIR DIST  ORDER
  1  2        2.232 0.401       2  3        1.225 1.675       3  4        1.077 0.881
  3  5        1.077 0.884

                          TOTAL        BONDED       FREE
   ATOM                   VALENCE      VALENCE      VALENCE
 1 AU                     0.471        0.471        0.000
 2 OXYGEN                 2.106        2.106        0.000
 3 CARBON                 3.486        3.486        0.000
 4 HYDROGEN               0.903        0.903        0.000
 5 HYDROGEN               0.906        0.906        0.000

     ------------------------------------------
     ATOMIC SPIN DENSITY AT THE NUCLEUS (A.U.)
     ------------------------------------------

                          SPIN DENS    ALPHA DENS   BETA DENS
 1 AU           19.0      0.0000000     0.00015      0.00015
 2 OXYGEN        8.0      0.0000000   145.47772    145.47772
 3 CARBON        6.0      0.0000000    59.13464     59.13464
 4 HYDROGEN      1.0      0.0000000     0.21413      0.21413
 5 HYDROGEN      1.0      0.0000000     0.21611      0.21611

     ---------------------
     ELECTROSTATIC MOMENTS
     ---------------------

POINT  1        X           Y           Z (BOHR)   CHARGE
             -1.754160  -0.965005   0.000000      1.00 (A.U.)
       DX        DY          DZ        /D/  (DEBYE)
   4.234728  -1.044573   0.000000   4.361657
 ..... END OF PROPERTY EVALUATION .....
 STEP CPU TIME =     0.04 TOTAL CPU TIME =      108.7 (   1.8 MIN)
 TOTAL WALL CLOCK TIME=      108.7 SECONDS, CPU UTILIZATION IS 100.00%
 222598 WORDS OF DYNAMIC MEMORY USED
 ddikick: all processes have ended gracefully.
  EXECUTION OF GAMESS TERMINATED NORMALLY Thu Sep 13 22:42:43 2001
 DATA SERVER STATS: TOTAL DISTRIBUTED MEMORY USED (MEMDDI)=       0 MWORDS.
 FIRST DATA SERVER'S MAXIMUM MEMORY=           0 WORDS, CPU=     0.0 SECONDS.
```

A3: Reference Absolute Energies (with Thermal Energy Corrections)

Table A1: Reference energies for calculation of relative energies.

Species	Energy (Hartrees)[1]
CO_2	-188.4030
H_2	-1.1580
H_2O	-76.3251
Cu^0	-196.0453
Cu^+	-195.7600
Zn^+	-65.2272
Au^0	-135.3736
Au^+	-135.0279

[1]A Hartree is equivalent to 2625.5 kJ/mol.

The use of M^0 or M^+ in M-CH_XOy was dictated by the overall charge of the molecule. For Zinc, however, Zn^+ was used in all calculations, due to its filled outer shell ([Ar] $3d^{10}$ $4s^2$ configuration).